AGU PUBLICATIONS

JGR

Journal of Geophysical Research: Atmospheres

RESEARCH ARTICLE
10.1002/2015JD023269

Key Points:
- Radiation management schemes cannot offset much more than 1.6 K of warming
- No radiation management schemes avoided regional precipitation changes
- Regional precipitation changes could potentially exceed changes under RCP4.5

Supporting Information:
- Figures S1–S5

Correspondence to:
J. A. Crook,
j.a.crook@leeds.ac.uk

Citation:
Crook, J. A., L. S. Jackson, S. M. Osprey, and P. M. Forster (2015), A comparison of temperature and precipitation responses to different Earth radiation management geoengineering schemes, *J. Geophys. Res. Atmos.*, *120*, 9352–9373, doi:10.1002/2015JD023269.

Received 24 FEB 2015
Accepted 11 AUG 2015
Accepted article online 14 AUG 2015
Published online 28 SEP 2015

A comparison of temperature and precipitation responses to different Earth radiation management geoengineering schemes

J. A. Crook[1], L. S. Jackson[1], S. M. Osprey[2], and P. M. Forster[1]

[1]Institute for Climate and Atmospheric Science, School of Earth and Environment, University of Leeds, Leeds, UK, [2]National Centre for Atmospheric Science, University of Oxford, Oxford, UK

Abstract Earth radiation management has been suggested as a way to rapidly counteract global warming in the face of a lack of mitigation efforts, buying time and avoiding potentially catastrophic warming. We compare six different radiation management schemes that use surface, troposphere, and stratosphere interventions in a single climate model in which we projected future climate from 2020 to 2099 based on RCP4.5. We analyze the surface air temperature responses to determine how effective the schemes are at returning temperature to its 1986–2005 climatology and analyze precipitation responses to compare side effects. We find crop albedo enhancement is largely ineffective at returning temperature to its 1986–2005 climatology. Desert albedo enhancement causes excessive cooling in the deserts and severe shifts in tropical precipitation. Ocean albedo enhancement, sea-spray geoengineering, cirrus cloud thinning, and stratospheric SO_2 injection have the potential to cool more uniformly, but cirrus cloud thinning may not be able to cool by much more than 1 K globally. We find that of the schemes potentially able to return surface air temperature to 1986–2005 climatology under future greenhouse gas warming, none has significantly less severe precipitation side effects than other schemes. Despite different forcing patterns, ocean albedo enhancement, sea-spray geoengineering, cirrus cloud thinning, and stratospheric SO_2 injection all result in large scale tropical precipitation responses caused by Hadley cell changes and land precipitation changes largely driven by thermodynamic changes. Widespread regional scale changes in precipitation over land are significantly different from the 1986–2005 climatology and would likely necessitate significant adaptation despite geoengineering.

1. Introduction

Global temperature change by the end of the 21st century is more likely than not to exceed 2°C relative to the 1850–1990 mean [*Intergovernmental Panel on Climate Change*, 2013], yet there has been a distinct lack of progress in mitigation efforts to reduce anthropogenic greenhouse gas emissions. Geoengineering Earth's climate by radiation management (RM) could potentially be deployed quickly once the technology is available and used to temporarily reduce the risk of adverse climate impacts [e.g., *Budyko*, 1977; *Crutzen*, 2006]. RM does not tackle climate change at its source but acts by reducing the solar radiation absorbed by the Earth's surface or by increasing the outgoing longwave radiation through means other than carbon dioxide removal, thereby reducing the net radiation input to the Earth's climate system at the top of the atmosphere. Proposed solar radiation management (SRM) schemes involve reflecting solar radiation away from the Earth in space, by aerosols injected into the stratosphere, by more reflective tropospheric clouds, or by enhanced Earth surface albedo. More recently a longwave radiation management (LRM) scheme has been suggested to reduce the amount of cirrus cloud so as to increase the outgoing longwave radiation at the top of the atmosphere [*Mitchell et al.*, 2008].

While SRM has the potential to stabilize global temperature [*Vaughan and Lenton*, 2011], the application of global SRM alone to return the Earth to its pre-industrial climate would result in the tropics being cooled too strongly and the Arctic too little [*Kravitz et al.*, 2013a] and would reduce precipitation too much with large regional changes in both directions [*Tilmes et al.*, 2013]. For the same surface temperature change, changes in net surface radiative fluxes caused by solar radiation changes are larger than those caused by terrestrial radiation changes; to balance the surface energy budget, changes in turbulent heat fluxes are also greater for solar radiation changes, making precipitation more sensitive to changes in solar radiation than to changes in terrestrial radiation [*Bala et al.*, 2008]. Furthermore, as demonstrated by *Haywood et al.* [2013] for stratospheric aerosol forcing and by *Muri et al.* [2014] for cirrus cloud thinning, differences in RM-induced cooling

between the Northern and Southern hemispheres have the potential to shift the location of the inter-tropical convergence zone (ITCZ) and change the spatial pattern of tropical precipitation. Although changes in the spatial pattern of tropical precipitation may be ameliorated by manipulation of the latitudinal and seasonal distributions of SRM [*MacMartin et al.*, 2013], this could prove challenging to deploy effectively in the real world [e.g., *Jackson et al.*, 2015].

The Geoengineering Model Intercomparison Project (GeoMIP) [*Kravitz et al.*, 2011] has been successful in assessing the robustness of regional effects of a reduction in solar irradiance to counteract a quadrupling of CO_2 [*Kravitz et al.*, 2013a] and also stratospheric SO_2 injection at a rate of 5 Tg SO_2 per year at the equator [*Yu et al.*, 2015] within a multimodel context. Yet there have been relatively few studies comparing the precipitation side effects of different RM schemes within a single model. *Jones et al.* [2011] showed there to be significant differences in regional climate between stratospheric SO_2 injection and sea-spray geoengineering: the radiative flux perturbation was more geographically uniform for stratospheric SO_2 injection than the regional sea-spray geoengineering, and regional patterns of cooling and precipitation change for stratospheric SO_2 injection more closely opposed the regional patterns of temperature and precipitation change from greenhouse gas warming. *Niemeier et al.* [2013] showed that the response of precipitation to sea-spray geoengineering was notably different to that due to stratospheric SO_2 injection or mirrors in space. These differences were explained by differences in the energy budget and Walker circulation changes. *Kalidindi et al.* [2015] showed that the climate responses from a reduction in solar constant and stratospheric aerosol injection were similar except for changes in stratospheric temperature, dynamics, and chemistry; and the partition between direct and diffuse solar radiation at the surface.

In this study, we compare the surface air temperature and precipitation responses of six different RM schemes simulated using the same climate model and the same simulation design, examining crop albedo modification, desert albedo modification, ocean albedo modification, sea-spray geoengineering, cirrus cloud thinning, and stratospheric SO_2 injections. These schemes were chosen to cover SRM intervention at different levels in the atmosphere and at the surface, and to have an example of LRM. The schemes involve manipulation of the Earth's radiation budget without directly addressing the increase in atmospheric greenhouse gas concentrations and so are classified as regional to planetary targeted climate modification [*Boucher et al.*, 2014].We took account of constraints on the scale or feasibility of RM schemes where evidence exists to support them: RM by reflectors in space was excluded because it would take many decades before a deployment would be fully operational [*Shepherd*, 2012]; crop and desert albedo modifications were constrained to grassland and desert regions and to albedo enhancements potentially achievable using current technology, although we sought to maximize their forcing within these constraints.

We use a fully coupled atmosphere-ocean general circulation model, a configuration of the UK Met Office HadGEM2 model, to simulate a projected future climate for the period from 2020 to 2099 assuming partial mitigation of anthropogenic climate change and apply individual RM schemes for 50 years from 2020. Our focus is on the temperature and precipitation changes during geoengineering, although we do consider rates of change immediately after the abrupt termination of RM and changes during the period 2080–2099, more than 10 years after the termination of RM. We do not consider other issues in the physical science. Social, political, ethical, and economic issues raised by the potential deployment of geoengineering, the handling of abrupt climate changes on termination, or being forced to continue geoengineering are also beyond the scope of this study.

2. Simulation Models and Methods

2.1. Climate Model Description

We used a fully coupled atmosphere-ocean general circulation model, a configuration of HadGEM2 [*Hardiman et al.*, 2012; *Martin et al.*, 2011], which includes processes for sea ice, ocean biogeochemistry, and the terrestrial carbon cycle, as well as a mass-based aerosol scheme for various aerosol species (sulfate, sea salt, black carbon, biomass-burning aerosols, mineral dust, fossil-fuel organic carbon, and secondary organic aerosol) [*Bellouin et al.*, 2007]. The Earth system components of HadGEM2 were diagnostic with the carbon cycle feedbacks turned off. The model does, however, include the effects of altered transpiration by stomatal resistance.

The model atmosphere has 60 vertical levels including 12 levels in the boundary layer. The model atmosphere extends to 84.5 km altitude, which provides enhanced representation of stratospheric dynamics and radiation compared to the low top version of HadGEM2, and a horizontal resolution of 1.25° latitude by 1.875° longitude. The model ocean has 40 vertical levels, a latitude resolution of 1° between the poles and 30°N/S increasing to 1/3° at the equator and a 1° longitude resolution.

The land-surface scheme, MOSES 2.2 [*Essery et al.*, 2001], handles subgrid heterogeneity by tiling. Each grid box may contain any of the following surface types: broadleaf trees, needleleaf trees, C3 (temperate) grass, C4 (tropical) grass, shrubs, urban, inland water, and bare soil. The albedos of these different types are derived from MODIS. The vegetation types are simulated by TRIFFID, a dynamical global vegetation model, which updates the plant distribution and soil carbon based on climate-sensitive CO_2 fluxes at the land-atmosphere interface every 10 model days [*Cox*, 2001]. The sulfate aerosol scheme [*Jones et al.*, 2001; *Bellouin et al.*, 2007] includes gaseous phase oxidation of SO_2 to H_2SO_4 in the stratosphere via reactions with the hydroxyl radical and stratosphere/troposphere aerosol gravitational sedimentation. Cloud microphysical processes are based on the scheme of *Wilson and Ballard* [1999]. Microphysical processes involving ice include nucleation, gravitational sedimentation, deposition, aggregation, riming, melting, and sublimation. Homogeneous nucleation of liquid water occurs at temperatures less than −40°C, and heterogeneous nucleation is active where temperatures are less than −10°C and vapor pressure exceeds a temperature-dependent threshold. Ice crystal fall speed is parameterized according to *Mitchell* [1996].

2.2. Simulation Design

Using HadGEM2, we produced one realization of 21st century climate for each of the six RM schemes and also for a control simulation. The simulations started on 1 January 2020 and continued to the end of 2099. The initial 1 January 2020 climate state was produced using a HadGEM2 simulation of natural and anthropogenic forcings for the period 1860–2005 and, for the period 2006–2019, greenhouse gas and aerosol concentrations from the Representative Concentration Pathway that produces a forcing of 4.5 W m^{-2} by 2100 (RCP4.5) [*Moss et al.*, 2010].

The control simulation was based on RCP4.5 with no RM geoengineering. RCP4.5 includes global emissions of greenhouse gases and short-lived species (CO_2, CH_4, N_2O, NO_x, VOCs, CO, SO_2, carbonaceous aerosols, HFCs, PFCs, NH_3, and SF_6), as well as land-use-land-cover changes. In order to reach this 4.5 W m^{-2} target, it includes implicit changes in the energy system, including the deployment of carbon capture and geologic storage technology [*Thomson et al.*, 2011].

For each RM scheme, we repeated the RCP4.5 simulation with RM of constant amount (see section 2.3 for details) starting in year 2020 and ending abruptly after 2069 as prescribed for the GeoMIP G4 scenario [*Kravitz et al.,* 2011]. In each case we targeted an effective radiative forcing (ERF) [*Myhre et al.,* 2013] of −2 W m^{-2} limited, in the case of crop albedo enhancement, by what could potentially be achievable in real world deployment. Our RM simulations did not return global mean temperatures back to the 1986–2005 climatology; therefore, we employed bias correction (section 2.4.3) to scale regional temperature and precipitation changes from our RM simulations before comparing them with the 1986–2005 regional climatology.

2.3. Simulation of the Geoengineering Schemes

2.3.1. Crop Albedo Enhancement (CROP)

An increase in the albedo of crops and grasslands could potentially contribute to a cooling of climate [*Ridgwell et al.*, 2009; *Doughty et al.*, 2011], although it is unlikely to achieve the scale of cooling that some other RM schemes may achieve. The albedo of different crops and grasses varies with plant color, waxiness, and morphology [e.g., *Doughty et al.*, 2011]. It has been suggested that selection of crop varieties to manipulate albedo could potentially increase crop albedo by 0.08 [*Ridgwell et al.*, 2009]. We simulated crop albedo enhancement by increasing the albedo of all C3 and C4 grasses, i.e., all grasslands including crops, by 0.08. In 2020, grassland covers 32.25 million km^2 (6.31% of the globe) in our model. This has reduced to 28.53 million km^2 (5.58% of the globe) by 2069, suggesting there is ~10% reduction in the forcing due to this feedback over the 50 years (see Figure S1 of the supporting information). Although beyond the scope of this study, the albedo enhancement from CROP could potentially be scaled up further by the development of bespoke genetically modified crops and grasses.

2.3.2. Desert Albedo Enhancement (DESERT)

Another proposal to increase land-surface albedo and cool climate is to site solar reflectors in desert regions [*Vaughan and Lenton*, 2011]. *Gaskill* [2004] has suggested using a reinforced highly reflective surface (e.g., polyethylene-aluminum), with an albedo of 0.8, to cover nonaeolian desert regions (currently ~11.7 million km^2). We simulated desert albedo enhancement by increasing bare soil albedo in desert regions to 0.8, the value also used by *Irvine et al.* [2011]. Our desert regions, defined to provide an ERF around $-2\,W\,m^{-2}$, were determined as being regions within 60°S to 60°N with no vegetation and having a bare soil albedo of more than 0.25 (bare soil albedo is dependent on soil color, so this selects regions with light soils typically found in deserts). This included the Sahara desert, Arabian desert, and large desert regions in Asia, Australia, and North America, covering a total of 18.63 million km^2 (3.64% of the globe) in 2020 and increasing the albedo of desert by 0.47 on average. Due to vegetation changes, this area reduced a small amount to 18.36 million km^2 (3.59% of the globe) by 2069, suggesting there is ~1% reduction in the forcing due to this feedback over the 50 years (see Figure S4). *Irvine et al.* [2011] applied desert albedo enhancement to a smaller desert land area of 9.1 million km^2.

2.3.3. Ocean Albedo Enhancement (OCEAN)

Ocean surface albedo could potentially be increased by the generation of microbubbles at the ocean surface, cooling climate [*Keith*, 2000; *Evans et al.*, 2010; *Seitz*, 2011]. We simulated ocean albedo enhancement by increasing albedo in HadGEM2 for all ice-free oceans (0.05–0.08 without geoengineering) by 0.03 to achieve an ERF of $\sim -2\,W\,m^{-2}$. In comparison, a calm ocean surface has an albedo in the range 0.05–0.10 [*Seitz*, 2011] and ocean bubbles in whitecaps have an albedo of 0.22 [*Moore et al.*, 2000]. This is a somewhat idealized simulation requiring bubble generation over a very large area; it gives a global scale forcing which is greater in the Southern Hemisphere than the Northern Hemisphere.

2.3.4. Sea-Spray Geoengineering (SEA-SALT)

It has been suggested that the climate could be cooled by increasing the albedo of marine stratocumulus clouds [*Latham*, 1990]. Sea salt aerosols could be injected into the marine boundary layer by spray of sea water from wind-powered ocean vessels [*Latham et al.*, 2008; *Salter et al.*, 2008]. If the sea-spray aerosols are uplifted into a relatively clean marine cloud layer, in which the availability of cloud condensation nuclei (CCN) is limited, the aerosols would strongly increase the availability of CCN. Under conditions of water vapor supersaturation, water vapor would condense onto these CCN resulting in an increase in cloud droplet number concentration and cloud albedo would be enhanced by the larger number of smaller cloud droplets [*Twomey*, 1977]. The reduction in cloud droplet size may also slow the coalescence of water droplets and reduce drizzle which would increase cloud liquid water content and further enhance cloud albedo [*Albrecht*, 1989].

We simulated sea-spray geoengineering by introducing a fixed increase in sea salt aerosol number concentration ($1.8 \times 10^8\,m^{-3}$) in the lowest atmospheric model level and then applied the same percentage change to the sea salt concentration in the next 11 vertical model levels to simulate the transport of sea salt within the boundary layer. We applied sea-spray geoengineering over the oceans between latitudes 30°N and 30°S, analogous to the GeoMIP scenario G4sea-salt [*Kravitz et al.*, 2013b].

Our approach has the advantage that it allows for both direct and indirect effects of increased sea salt aerosol concentrations (unlike simulations that apply a fixed increase to cloud droplet number concentration), and it targets the most effective regions for sea-spray geoengineering [*Jones and Haywood*, 2012]. It falls short, however, of the GeoMIP G4sea-salt specification in that we do not simulate the emission of sea salt aerosols and their transport within the marine boundary layer.

2.3.5. Cirrus Cloud Thinning (CIRRUS)

It has been suggested that thinning cirrus clouds could cool the climate [*Mitchell et al.*, 2008]. In relatively cold cirrus cloud formation regions (<235 K), with low concentrations of aerosols, the formation of ice crystals in cirrus clouds is dominated by homogeneous nucleation in which water vapor molecules cluster together and freeze in the atmosphere [e.g., *Karcher and Lohmann*, 2002]. Seeding these regions with an efficient ice nucleating compound (e.g., bismuth tri-iodide) could promote heterogeneous nucleation in which water vapor freezes on the surface of the ice nucleating aerosols [*Mitchell and Finnegan*, 2009]. This would accelerate the freezing process and lead to the growth of larger ice crystals which would fall more quickly than the smaller crystals produced by homogeneous nucleation. The increase in ice crystal fall speed would deplete the cirrus cloud of ice and deplete the humidity of the surrounding atmosphere.

Climate model simulations have shown that such cirrus cloud thinning would increase outgoing longwave radiation at top of atmosphere, reduce reflected shortwave radiation, and yield a net negative radiative forcing [*Sanderson et al.*, 2008; *Storelvmo et al.*, 2013]. Following the approach of *Muri et al.* [2014], we adopted a simplified representation of cirrus cloud seeding in HadGEM2 in which we increased the model ice crystal fall speed parameter. To achieve an ERF of $-2\,W\,m^{-2}$, we quadrupled ice crystal fall speed globally for air temperatures colder than 233 K (see Figure S1), effectively focusing our efforts on regions of homogeneous ice nucleation [doubling ice crystal fall speed, as in *Muri et al.*, 2014, produced an ERF of only $-1\,W\,m^{-2}$].

2.3.6. Stratospheric SO_2 Injection (SULFATE)

The injection of aerosols or their precursor gases into the stratosphere could mimic the cooling effect of explosive volcanic eruptions through backscatter of incoming solar radiation [*Robock*, 2000]. One potential candidate for stratospheric aerosol formation is SO_2 gas. It could be injected into the lower stratosphere, for example, by tanker aircraft, where it would react with water and hydroxyl radicals to form sulfate aerosols with a size distribution effective at scattering incoming shortwave radiation and producing a cooling effect on climate. We simulated the injection of SO_2 into the tropical stratosphere in HadGEM2 at an altitude of 16 km to 25 km over the equator and at a rate of 10 Tg SO_2 yr^{-1}. This is at the upper end of what has been proposed in previous studies (from 1 Tg S yr^{-1} to 5 Tg S yr^{-1}) [*Lenton and Vaughan*, 2009] and double that defined by the GeoMIP G4 scenario [*Kravitz et al.*, 2011]. However, we found that 5 Tg SO_2 yr^{-1} produced an ERF of only $-0.5\,W\,m^{-2}$ and a global mean temperature change in 2040–2059 of only -0.4 K. This temperature reduction is relatively small compared to the -0.83 K change produced by *Jones et al.* [2011] when simulating a 2.5 Tg S yr^{-1} injection using a HadGEM2 model with only 38 vertical levels in the atmosphere, and uniformly distributing the SO_2 initially. The weaker forcing from our model is likely due to changes in the lifetime and latitudinal distribution of sulfate aerosols that arise from simulation of the Brewer-Dobson circulation at an enhanced model resolution and height, and also the inclusion of gravitational settling of stratospheric sulfate aerosol.

2.4. Analysis of Results

2.4.1. Determination of Effective Radiative Forcing

To determine the ERF for each RM scheme we used the method of *Gregory et al.* [2004], regressing global mean top of atmosphere radiative flux anomalies (geoengineering−RCP4.5) against global mean surface air temperature anomalies. For the schemes where reductions in temperature had largely occurred within 10 years, we regressed over the first 10 years, and for the schemes where reductions in temperature took closer to 20 years (DESERT and OCEAN), we regressed over the first 20 years. The slope of the regression line gives the feedback parameter, and the intercept gives the ERF. Radiative fluxes were broken down into their components, shortwave (sw), longwave (lw), and clearsky (cs). We also applied the method to zonal means to determine the zonal mean ERF components.

2.4.2. Analysis of Temperature and Precipitation Responses

To assess the magnitude of the response to geoengineering, we compared the difference between 20 year means from our geoengineering simulations (2040–2059), the control simulation (2040–2059), and the last 20 years of the Coupled Model Intercomparison Project Phase 5 (CMIP5) [*Taylor et al.*, 2012] historical climate simulation (1986–2005). The 2040–2059 time period was chosen to compare the geoengineering simulations with the control simulation because first, temperature responses to the RM schemes had ceased cooling relative to RCP4.5; and second, global annual mean temperatures were closest to the 1986–2005 climatological mean for many of the RM schemes which was advantageous for minimizing the extent of bias correction (see section 2.4.3).

We determined the statistical significance of a change in temperature or precipitation by comparison to internal variability. We estimated internal variability by calculating the standard deviation of nonoverlapping 20 year means from the last 400 years of a 500 year pre-industrial control run following *Collins et al.* [2013]. We used this method to capture low frequency climate variability and used 20 year means so that there were sufficient mean values (i.e., at least 20) to constrain the uncertainty of the calculated standard deviations. The internal variability was multiplied by $\sqrt{2}$ as we are testing the significance of the difference between two means. This internal variability is hereafter referred to as SD20. Statistical significance was measured at the 5% significance level, using two standard deviations as an approximation of the critical value for a two-tailed *t*-test.

In sections 3.1 and 3.3.1, we present changes in global annual means and the ratio of the change in annual mean temperature over land to the change in annual mean temperature over sea. We used a fixed land-sea

mask to calculate this ratio and treated the Arctic Ocean, whether covered in sea ice or open to the atmosphere, as sea.

In sections 3.3.2 and 3.4 we present 2040–2059 maps of the changes in surface air temperature and precipitation, respectively, so we can compare changes in regional annual means for the schemes. We apply the energy budget analysis of *Muller and O'Gorman* [2011] to understand regional changes in precipitation. The surface precipitation flux can be equated to the column-integrated diabatic cooling (Q), excluding latent heating, and the column-integrated divergence of dry static energy (H), such that changes in precipitation ΔP are given by

$$L_c \Delta P = \Delta Q + \Delta H \tag{1}$$

The ΔQ term can be calculated from changes in the net upward top of atmosphere radiative fluxes (R_{TOA}), the net upward surface radiative fluxes (R_S), and the net upward surface sensible heat fluxes (SH) by

$$\Delta Q = \Delta R_{TOA} - \Delta R_S - \Delta SH \tag{2}$$

In section 3.5 we assess how effective each scheme is at bringing the climate back to the 1986–2005 climatology. This target was set as an approximation to the late 20th century climate. Other choices are available and equally plausible, and our results will reflect, in part, our choice of climatology. To understand effectiveness we need to assess changes caused by the geoengineering in context with changes in RCP4.5 compared to climatology. We use a form of bias correction to scale the 2040–2059 global annual mean surface air temperature to match the 1986–2005 climatological temperature. Our simulations were closest to the 1986–2005 climatology in 2040–2059.

2.4.3. Bias Correction

Bias correction has been used in a previous geoengineering comparison [*Niemeier et al.*, 2013]. Here we assume that the amount of forcing for all but CROP and DESERT can be increased (response linearly scaled up) or decreased (response linearly scaled down) to scale the global annual mean surface air temperature back to the 1986–2005 climatological global annual mean. Within the twin constraints of current technology and land use, CROP and DESERT forcings are at their maximum so the response can only be scaled down, but we find CROP needs to be scaled up and we, therefore, do not bias correct in this case. We apply a scaling factor α such that

$$\alpha = \frac{\overline{\Delta T_{RCT} - \text{clim}}}{\Delta T_{geo} - \text{RCP}} \tag{3}$$

where overbar indicates a global mean and temperature differences are the means over the 2040–2059 period. The scaled 2040–2059 annual mean surface air temperature for each model grid cell is given by

$$T_{geo,scaled} = \alpha \Delta T_{geo\text{-}RCP} + T_{RCP} \tag{4}$$

where the same value for α is used for all grid cells. We use the same scaling factor to bias correct the global annual mean temperature when analyzing effectiveness of precipitation responses. We are assuming that the forcing can be linearly scaled up or down such that the global annual mean temperature equals the climatological mean and the regional temperature/precipitation response patterns remain the same. Note that we bias correct for global mean temperature but we could have equally chosen to bias correct for global mean precipitation. We discuss bias correction for global mean precipitation in section 3.6.

3. Results

3.1. No Geoengineering Control Simulation (RCP4.5)

Without geoengineering, the global annual mean surface air temperature in the RCP4.5 simulation increases by 1.61 K by 2046–2065 compared to the 1986–2005 climatology, within the one standard deviation range for the CMIP5 climate model ensemble projections (+1.4 ± 0.3 K) [*Collins et al.*, 2013]. The increase in global annual mean surface temperature by 2040–2059 is 1.50 K [Figure 1(a)] compared to the 1986–2005 climatology. Warming is greatest over high northern latitudes and over land. The ratio of warming over land to warming over sea is 1.69. Warming occurs virtually everywhere, and by 2040–2059, the land warming is more than 4 standard deviations (SD20) from the 1986–2005 climatology over most of the globe and more than 10 standard deviations from the 1986–2005 climatology over much of the tropics [Figure 1(b)]. The Arctic

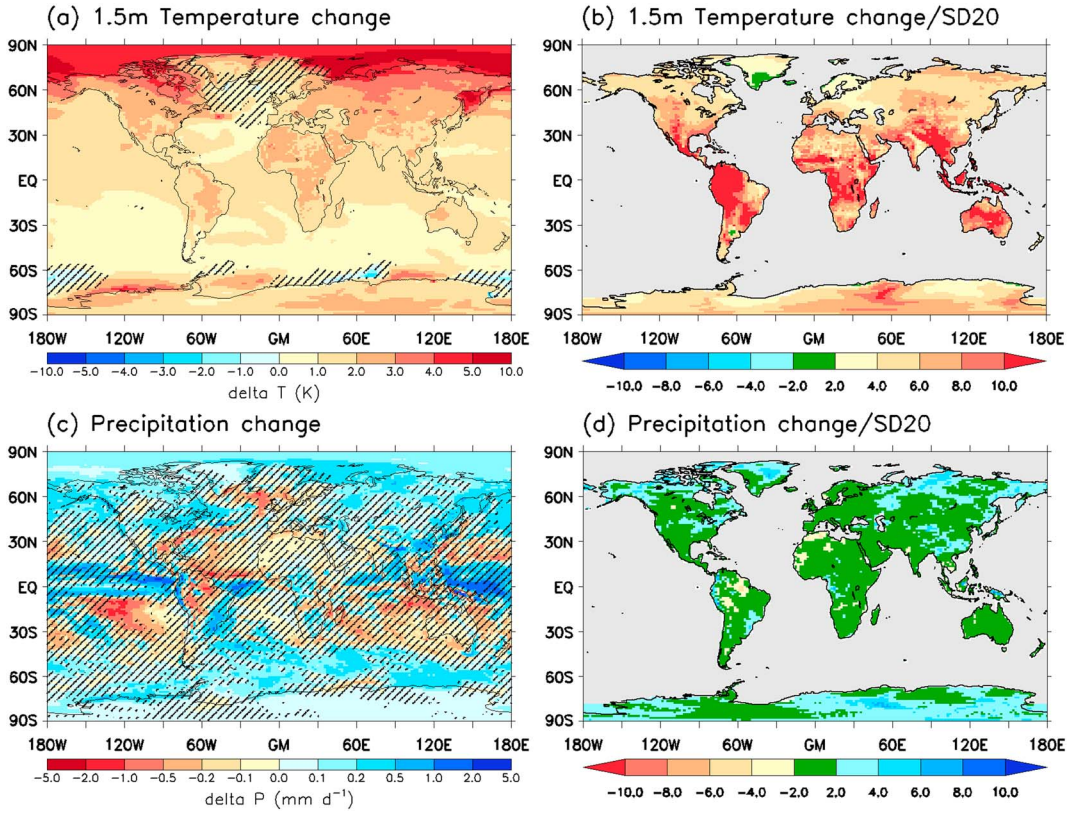

Figure 1. RCP4.5 scenario 2040–2059 mean changes in surface air temperature and precipitation compared to 1986–2005 climatology expressed as absolute values [(a) in K and (c) in mm d^{-1}] and as number of standard deviations (SD20) for land only [(b) and (d)]. Hatching in Figures 1(a) and 1(c) show regions where changes are not significant at the 5% significance level.

amplification defined as $\Delta T_{60-90N}/\Delta T_{global}$ for 2040–2059 is 2.05, and the Antarctic amplification defined similarly but for the Southern Hemisphere is 1.24.

Precipitation increases globally by 0.07 mm d^{-1} (2.2 %) by 2040–2059 [Figure 1(c)] compared to the 1986–2005 climatology, slightly more over sea than land, and the largest changes occur over the tropical sea. By 2040–2059, land precipitation changes are still within 2 standard deviations (SD20) of the 1986–2005 climatology over much of the globe but can be more than 4 standard deviations different in a few regions [Figure 1(d)].

3.2. Estimated ERF

Our estimated global mean ERF components are shown in Figure 2, the net forcing is given in Table 1, and the regression plots are shown in Figure S2. The net forcing is considerably smaller for CROP than the other RM

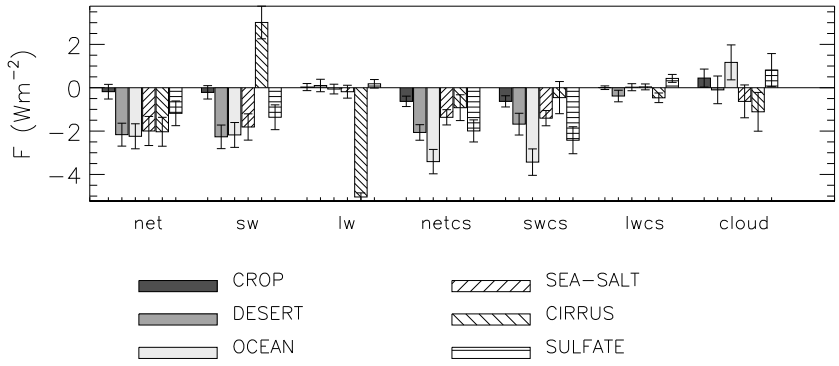

Figure 2. Global mean ERF components in W m^{-2}. Error bars show ±2 standard deviations determined from the regression.

Table 1. Global Mean ERF (±2σ) for Geoengineering Less RCP4.5, 2040–2059 Mean Surface Air Temperature Change, Transient Climate Sensitivity, Land-Sea Temperature Change Ratio, Polar Amplification, and Bias Correction Scaling Factor for Each RM Scheme

					Polar Amplification		Bias Correction α
	F_{net} (W m^{-2})	$\Delta T_{2040-59}$ (K)	Transient Climate Sensitivity (K W^{-1} m^2)	$\Delta T_{land}/\Delta T_{sea}$	60–90°N	60–90°S	
CROP	−0.18 ± 0.34	−0.18	0.97 ± 1.78	2.4	2.38	0.33	N/A
DESERT	−2.17 ± 0.53	−1.65	0.76 ± 0.19	4.7	1.59	0.08	0.91
OCEAN	−2.24 ± 0.58	−1.57	0.70 ± 0.18	1.4	2.05	0.87	0.96
SEA-SALT	−2.00 ± 0.67	−0.97	0.49 ± 0.16	1.5	1.84	0.60	1.54
CIRRUS	−2.03 ± 0.67	−1.04	0.51 ± 0.17	1.8	2.38	1.45	1.44
SULFATE	−1.18 ± 0.57	−0.92	0.78 ± 0.37	1.7	1.57	0.71	1.65

schemes and, although negative in the global mean, is positive in some regions. Rapid cloud adjustments make a significant and opposing difference to the forcing of RM schemes that did not intentionally modify clouds, i.e., CROP, DESERT, OCEAN, and SULFATE. For SEA-SALT the direct effect (sw clear sky component) and the indirect effect from brightening the cloud (cloud component) are both negative. For CIRRUS the large negative lw forcing from thinning the cloud is reduced considerably by the fact that more sw can now reach the surface. For all other RM schemes, the lw forcing is small.

Figure 3 shows there are distinct patterns of zonal mean ERF for the different RM schemes, particularly for DESERT where the net forcing is strongly negative in the Northern Hemisphere tropics (Sahara desert) and positive in the Southern Hemisphere tropics. For DESERT we found very large rapid reductions in cloud and water vapor just north of the equator and the opposite just south of the equator, amplifying the contrast in net forcing on either side of the equator and also seen in the lw forcing. For SEA-SALT the sea salt injection was restricted to the tropics and the forcing is seen mostly in this region, whereas sea albedo changes were applied everywhere and so the negative net forcing of OCEAN extends into the extratropics. For CIRRUS the negative net forcing is largest in the extratropics (in the tropics the sw forcing is more effective at counteracting the lw forcing because of the large incoming sw here). For SULFATE the net negative forcing is largest close to the equator. We found the SO_4 aerosol had a maximum concentration near the equator throughout the geoengineering period so had not spread as effectively as has been assumed for low top HadGEM2 simulations or was found for the GISS model E [*Jones et al.*, 2010]. This may, in part, be related to the SO_4 aerosol lifetime which has been shown to depend on both the injection rate [*Heckendorn et al.*, 2009] and injection height [*Niemeier et al.*, 2011]. The lw forcing is positive just south of the equator and negative just north of the equator for all RM schemes except CIRRUS, where the lw forcing is negative on both sides of the equator but more negative just north of the equator. Deep tropical convection gives rise to a large amount of cirrus in this region.

3.3. Surface Air Temperature Response

3.3.1. Global Temperature Changes

Figure 4 shows the global annual mean surface air temperature time series, over the whole globe, land only and sea only for each RM scheme and for RCP4.5. RCP4.5 shows an almost linear trend in global annual mean temperature over the years 2020–2099 (+0.20 ± 0.01 K decade^{-1}). All RM schemes show a reduction in temperature over the first 10 to 20 years, and thereafter, they track RCP4.5 until termination when temperature returns to the RCP4.5 state within about 5 years. Temperature responses are greater over land than sea particularly for DESERT which has a 2040–2059 land-sea temperature change ratio of 4.7 (see Table 1). OCEAN and SEA-SALT have the lowest 2040–2059 land-sea temperature change ratios because the instantaneous forcing is applied over the sea. SULFATE has the closest land-sea temperature change ratio to RCP4.5 which makes sense because the other RM schemes have greater geographical heterogeneity.

For CROP the global mean temperature response is very small. This scheme could at best be used to reduce warming locally and deliver local scale benefits to soil moisture and primary productivity [*Singarayer et al.*, 2009]. It is also unlikely that the global mean temperature can be brought back within our 1986–2005 climatology for much more than 50 years for any of the other RM schemes unless the level of intervention could be increased significantly. This would not be possible for DESERT as we are using the maximum forcing possible. It may also not be possible for SEA-SALT because we found little variation in temperature response for boundary layer concentrations of sea salt ranging from 1.4×10^8 m^{-3} to 2.0×10^8 m^{-3}.

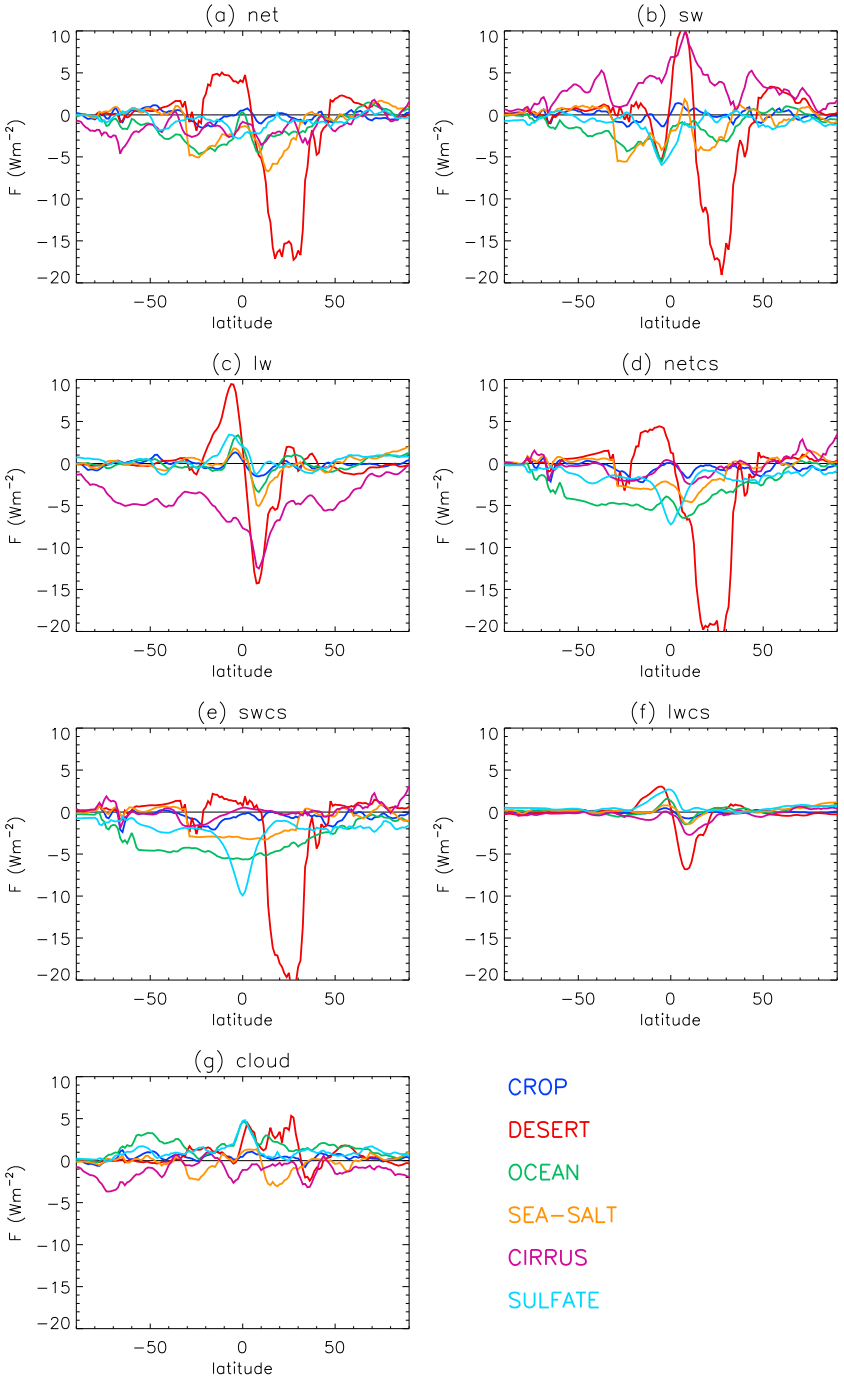

Figure 3. Zonal mean ERF components in W m^{-2}.

However, *Kravitz et al.* [2013b] have shown ERF to be linear around −2 W m^{-2} in GeoMIP G4 sea-spray geoengineering simulations. This suggests that we require more precise estimates for ERF over a wider range of sea salt concentrations before we can conclude that the cooling capability of sea-spray geoengineering is limited to around −1 K as in our results.

For CIRRUS, however, we suggest that ERF cannot be increased much further and that its cooling capability is indeed limited to little more than the −1 K in our results. We found ERF at the top of atmosphere did not continue to increase with an increase in ice crystal fall speed (Figure S3). Although our standard errors for the ERF were large for CIRRUS, *Storelvmo et al.* [2013] have shown cloud radiative forcing from cirrus cloud thinning to

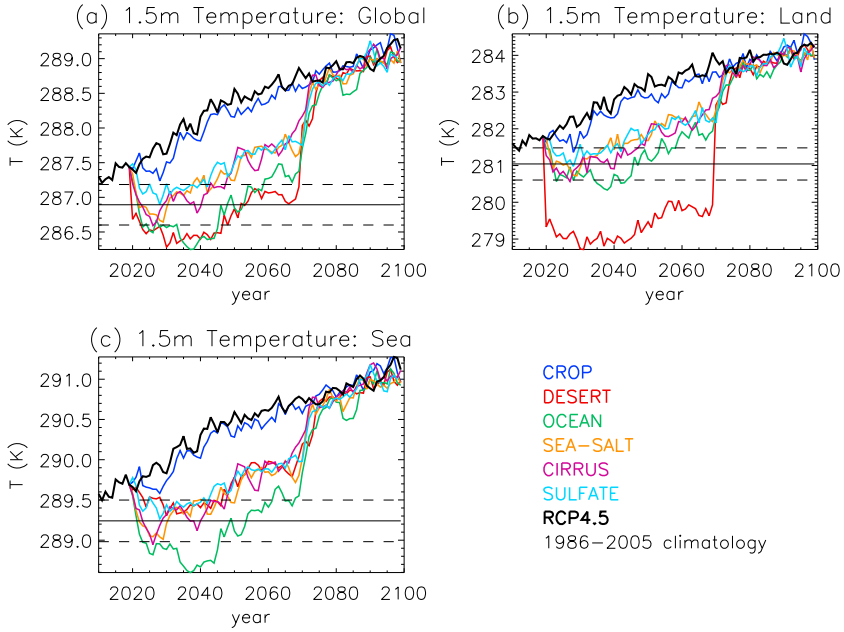

Figure 4. Global mean surface air temperature time series in K. The horizontal black line shows the 1986–2005 climatology with the dashed horizontal lines showing ±2 annual mean standard deviations of the pre-industrial control run.

be sensitive to the seeding ice nuclei concentration and limited to a maximum of $-2\,\mathrm{W\,m^{-2}}$. We cannot comment on whether increasing stratospheric SULFATE emissions in our model would significantly increase the amount of cooling. The atmospheric aerosol burden and the forcing from stratospheric SO_2 injection do not increase linearly with the amount injected due to coagulation and fall out of particles [*Heckendorn et al.*, 2009] which are also a function of concentration and injection rate.

The global mean temperature anomalies from RCP4.5 for 2040–2059 are shown in Table 1. Generally, the larger the forcing, the larger the global mean temperature change. However, the transient climate sensitivity (defined here as $\Delta T_{2040-2059}$ divided by ERF) is greater for the surface albedo modification schemes and SULFATE than for schemes that modify clouds in the troposphere. We found the net zonal mean feedback for SEA-SALT and CIRRUS to be significantly more negative around 30°S and 20°N than that for the other RM schemes resulting in a smaller temperature change for the same forcing. This is likely due to the different forcing patterns, the distribution of cloud cover across the tropics, and rapid cloud adjustments (cloud forcing in the tropics is negative for SEA-SALT and CIRRUS and positive for the other schemes).

3.3.2. Regional Temperature Changes

To aid the comparison of regional temperature responses from the alternative geoengineering simulations, we calculated the ratio of the temperature change in each grid cell to the change in global annual mean temperature (Figure 5). CROP and DESERT are more regional interventions and show distinct temperature response patterns. CROP cools the grassland regions but also cools high latitudes particularly in the Northern Hemisphere and warms the Southern Ocean, although changes are largely insignificant. DESERT has severe cooling in the Sahara desert (−27 K), and mostly cools the Northern Hemisphere and warms parts of the Southern Hemisphere ocean. OCEAN, SEA-SALT, CIRRUS, and SULFATE have similar temperature response patterns, with spatial pattern correlation coefficients between pairs of these schemes lying between 0.64 and 0.88. These schemes are more effective at providing a global response (virtually all regions are significantly cooler than RCP4.5 at the 5% significance level). Previous studies have shown that SRM tends to cool the tropics too much and the Arctic not enough [*Kravitz et al.*, 2013a]. Of the more effective global RM schemes, we find SEA-SALT and SULFATE have the lowest polar amplifications (lower than RCP4.5) and CIRRUS has the highest (even higher than RCP4.5) (see Table 1). This is not surprising given the net forcing is more concentrated in the tropics for SEA-SALT and SULFATE than the net forcing of CIRRUS which is more evenly distributed across the tropics and the midlatitudes (Figure 3). Differences in meridional heat transport may also play a role [e.g., *Crook et al.*, 2011].

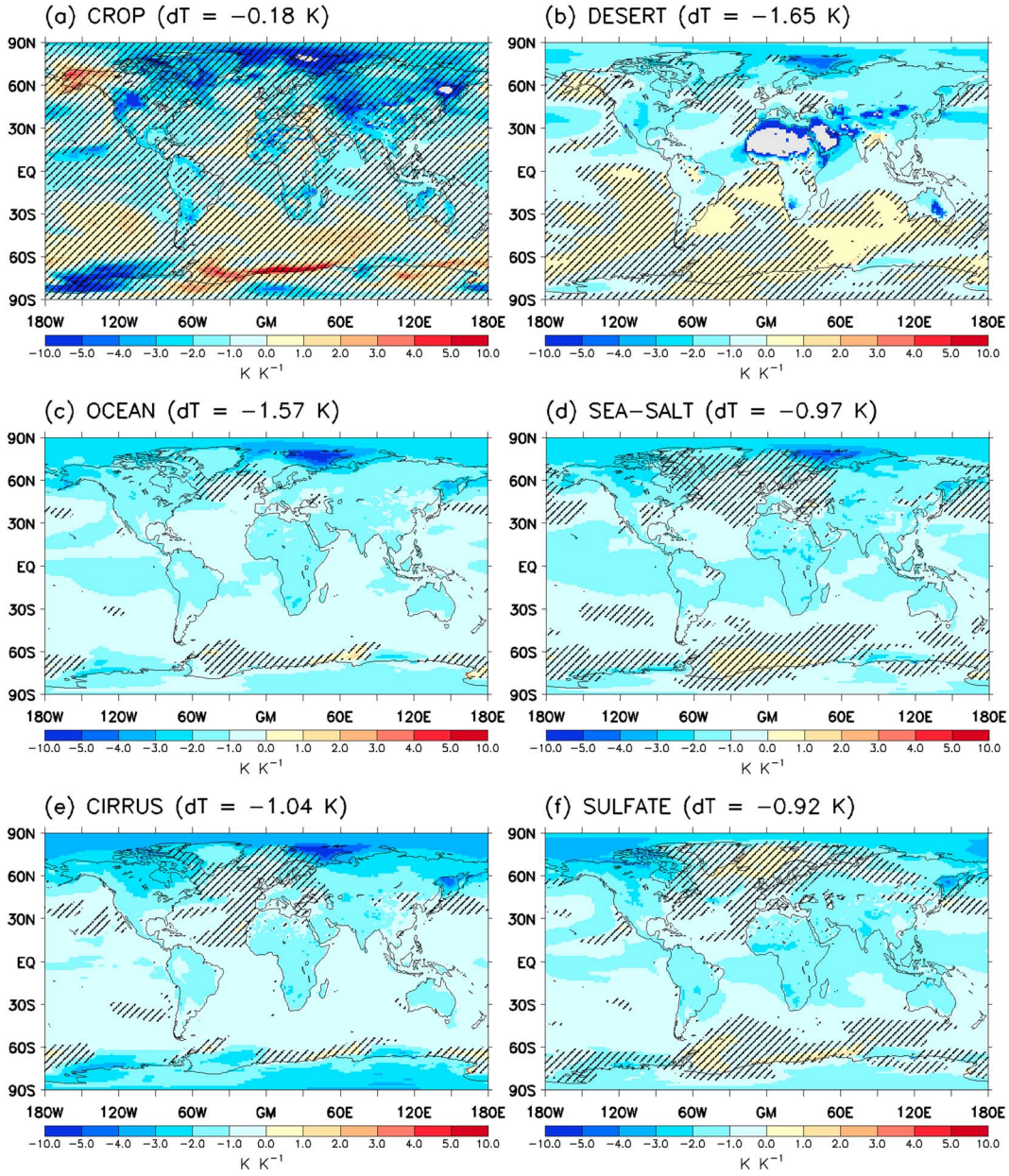

Figure 5. Ratio of the change in regional surface air annual temperature to the change in the global annual mean temperature change (shown in each title) in K K^{-1} for each of the geoengineering schemes. The changes are compared to RCP4.5 (2040–2059 mean). Hashed areas are not significant at the 5% significance level based on SD20.

3.3.3. After Termination of Geoengineering

Figure 4 shows that over the 5 years after termination of geoengineering, there are very rapid rates of temperature change (~0.2 K yr^{-1}). This is around 10 times the linear rate of change over the whole of the 21st century in RCP4.5. *Jones et al.* [2013] analyzed a multimodel ensemble of GeoMIP G2 simulations: They compared the rate of warming during the decade after terminating geoengineering to the rate of warming during a 70 year simulation of forcing from 1% per annum increase in the concentration of CO_2 and found global temperature warmed 4.1 ± 1.2 times faster after terminating geoengineering; during the decade after terminating geoengineering in SULFATE, we found global temperature warmed 4.0 times faster than the warming from RCP4.5. *Alterskjær et al.* [2013] simulated sea-spray geoengineering in three climate models using a GeoMIP G3 simulation design: they found global temperature warmed 0.73°C after termination of geoengineering; we found global temperature warmed 1.11°C after termination of geoengineering in SEA_SALT.

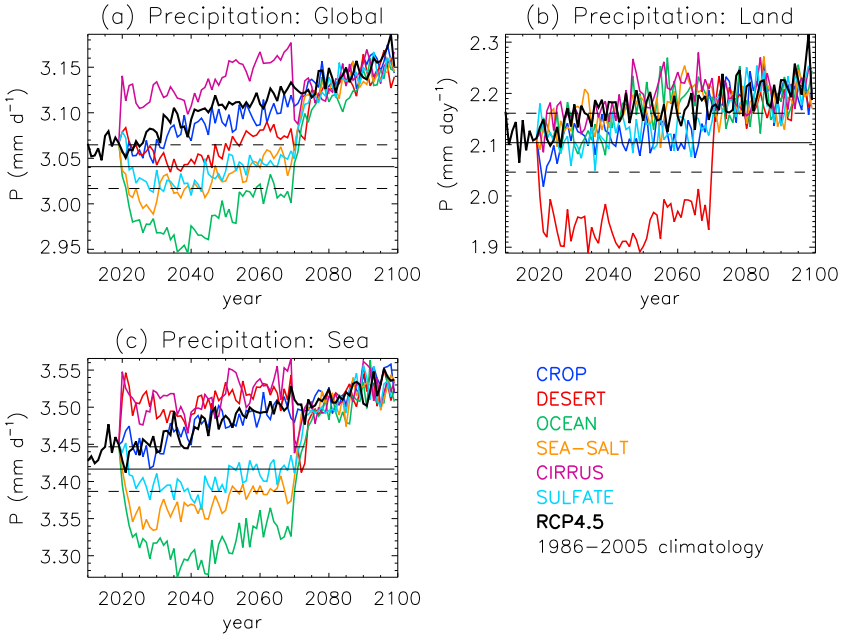

Figure 6. Global mean precipitation intensity time series in mm d^{-1}. The horizontal black line shows the 1986–2005 climatology with the dashed horizontal lines showing ±2 annual mean standard deviations of the pre-industrial control run.

Regionally, much larger rates of temperature change occur over the 5 years after termination (over 0.5 K yr^{-1} in many regions and even more than 1 K yr^{-1} in some places for some RM schemes). The larger the temperature change caused by the geoengineering, the larger the rates of change after termination. Although globally the temperature returns to RCP4.5 within around 5 years, regionally this may take considerably longer. Maps of the temperature difference between geoengineering schemes and RCP4.5 averaged over the 2080–2099 period and expressed as a number of standard deviations (SD20) (Figure S4) show that most of the land has returned to RCP4.5 within ±2 standard deviations (SD20), and all has returned to within ±4 standard deviations (SD20).

3.4. Precipitation Response

3.4.1. Global Precipitation Changes

Figure 6 shows the global mean precipitation time series, over the whole globe, land only and sea only for each RM scheme and for RCP4.5. RCP4.5 shows an almost linear increase in precipitation over the century. All RM schemes except CIRRUS show a decrease in precipitation over the first 10 to 20 years, while the temperature is cooling due to there being less evaporation in a cooler world, and thereafter, they track RCP4.5 (i.e., increasing precipitation) until termination when precipitation returns to the RCP4.5 state within about 5 years. For CIRRUS, there is an immediate increase in precipitation which is likely a rapid adjustment [*Myhre et al.*, 2013] in which the increased radiative cooling of the atmosphere is balanced by an increase in latent heat flux, and therefore precipitation, as illustrated by *Andrews et al.* [2009] for many different forcing mechanisms. Thereafter, CIRRUS follows the pattern of the other RM schemes but always has greater precipitation than RCP4.5 because the initial adjustment is so strong compared to the feedback response with temperature. The precipitation changes for all but CROP and DESERT are found to occur mostly over the sea, with global mean land showing very small changes in precipitation. DESERT behaves quite differently with a rapid increase in maritime precipitation but a very large decrease in land precipitation which dominates the global mean.

3.4.2. Regional Precipitation Changes

To aid the comparison of regional precipitation responses from the alternative geoengineering simulations, we calculated the ratio of the precipitation change in each grid cell to the change in global annual mean temperature (Figure 7).

CROP reduces sw absorption over the modified grassland which causes reduction of evapotranspiration and therefore precipitation in those regions. However, precipitation changes are also seen elsewhere but are mostly not significant at the 5% significance level.

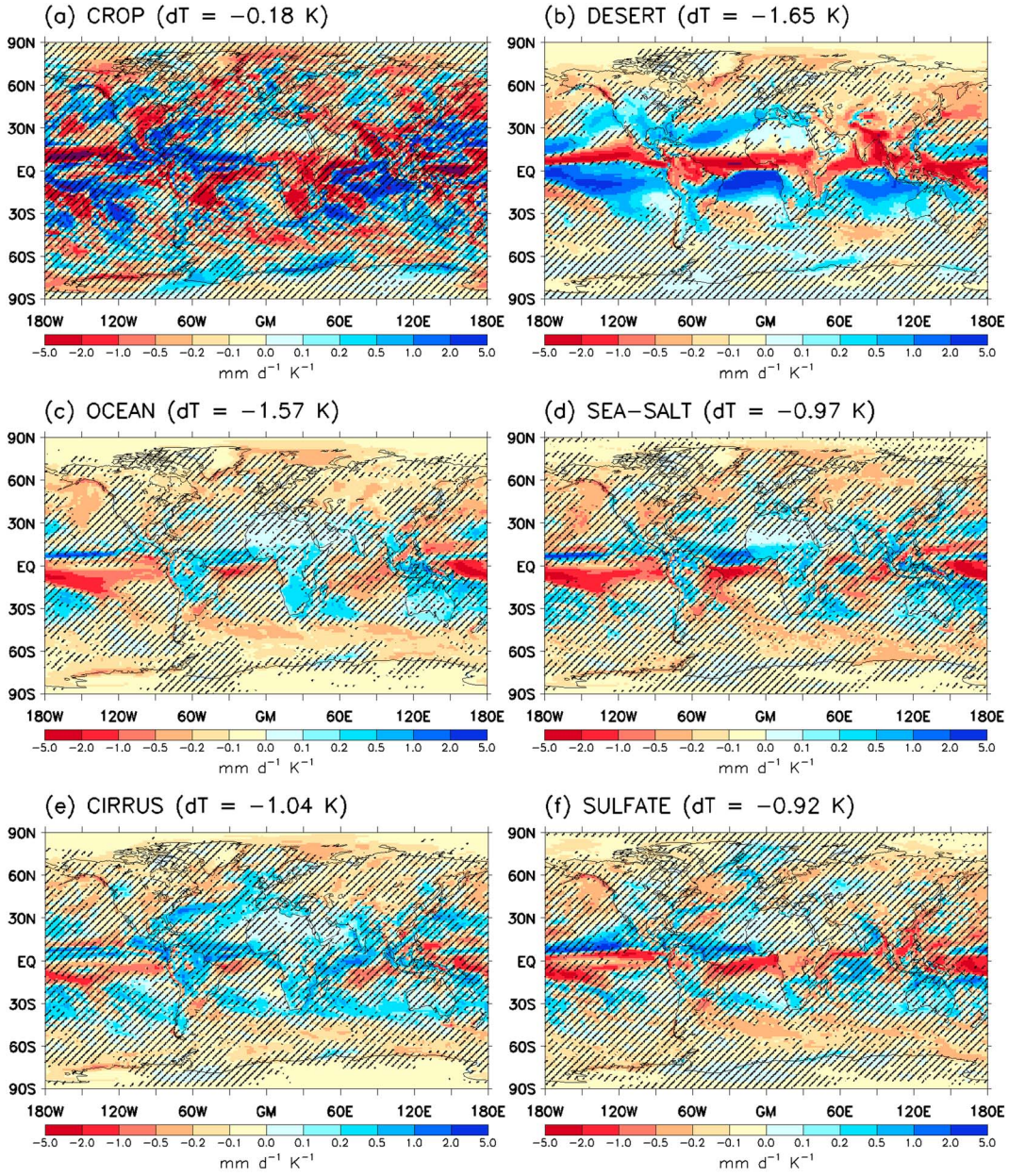

Figure 7. Ratio of the change in regional precipitation intensity to the change in global annual mean temperature change (shown in each title) in mm d^{-1} K^{-1} for each of the geoengineering schemes. The changes in precipitation intensity and temperature were compared to RCP4.5 (2040–2059 mean). Hashed areas are not significant at the 5% significance level based on SD20.

DESERT shows large shifts in tropical precipitation. The mean latitude weighted by precipitation between 30° north and south of the equator changed from 0.2°S to 2.0°S. Extreme reductions occur over northern South America, the Sahel, India, and parts of China, and there is more rainfall just south of the equator, similar to the results of *Irvine et al.* [2011]. This change in tropical precipitation is accompanied by large regional temperature changes with reductions in cloud and water vapor just north of the equator and very large increases in cloud and water vapor just south of the equator. We also found large changes to the Hadley cell (diagnosed from changes in 500 hPa vertical velocity) with enhanced upward motion just south of the equator increasing the local precipitation and reduced upward motion just north of the equator decreasing the local precipitation (Figure 8). These changes in upward motion occur in all seasons, changing the intensity of vertical motion but not so much that the seasonal cross-equatorial migration of the upward branch of the Hadley cell

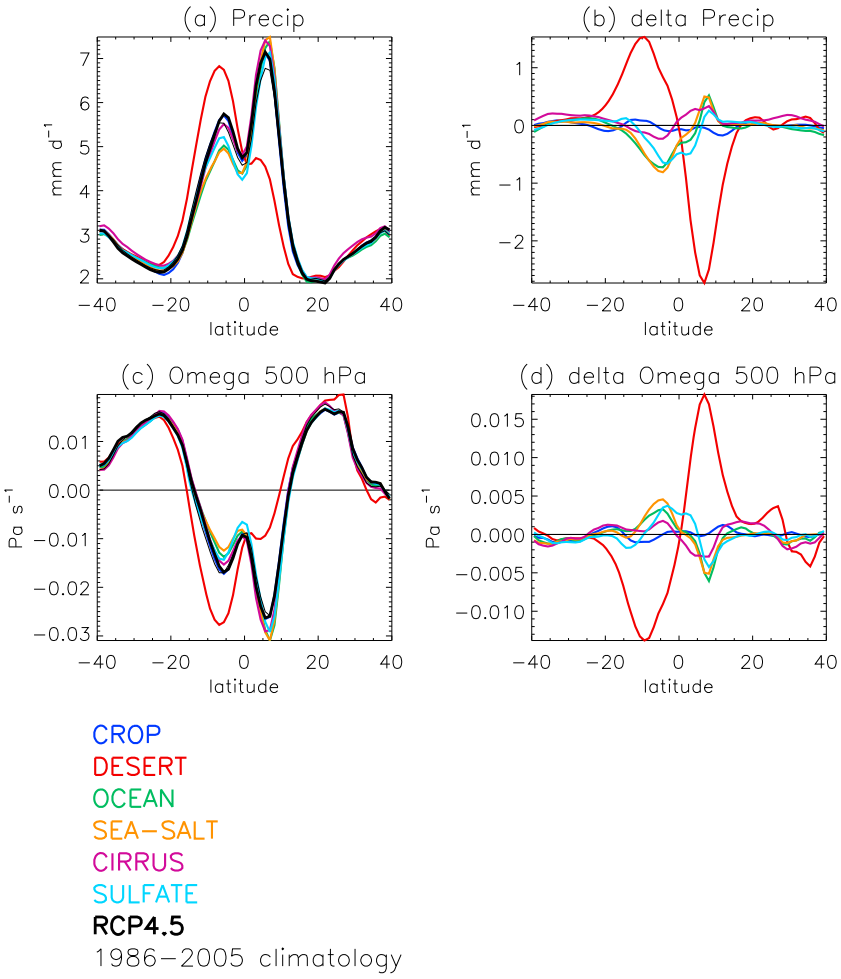

Figure 8. (a) 2040–2059 zonal mean tropical precipitation intensity in mm d^{-1}, and (c) 500 hPa omega in Pa s^{-1} for RCP4.5 and the different geoengineering schemes, and (b) changes in precipitation intensity and (d) changes in 500 hPa omega for the different geoengineering schemes compared to RCP4.5.

is inhibited. These changes occur within 5 years of starting geoengineering and are maintained throughout the geoengineering period.

For OCEAN, SEA-SALT, CIRRUS, and SULFATE the largest changes occur in the tropics, particularly over the sea, with a decrease occurring just south of the equator and an increase to the north (Figure 7). This pattern looks remarkably similar for these different schemes. The spatial pattern correlation coefficients over the whole globe between pairs of these schemes lie between 0.65 and 0.85 not including SULFATE and between 0.40 and 0.61 for correlations with SULFATE. The ascending branch of the Hadley cell shifts northward; this results in an increase in precipitation just north of the equator and a decrease to the south (Figure 8). Although these changes are much greater over the sea, the Amazon and Sahel are also affected and so are particularly vulnerable to precipitation change for all RM schemes. OCEAN, SEA-SALT, CIRRUS, and SULFATE also show similar responses over many land areas, e.g., increase in northwest US, decrease in southeast US, decreases over large parts of Eurasia, increase in southwest Europe, increases in large parts of Africa, decrease in Uruguay, and increase in Australia. These responses are mostly of opposite sign to the response of the RCP4.5 simulation compared to climatology, but the magnitudes are such that the different RM schemes are not always able to return the local precipitation to the climatology. For SULFATE, central Africa has a notable decrease compared to other RM schemes. For SEA-SALT, there is a considerable decrease in the Amazon region not seen in OCEAN and CIRRUS, and seen to a much lesser degree in SULFATE. Given that we only have one ensemble member for all RM schemes, it is difficult to say whether the more subtle differences between schemes are because of

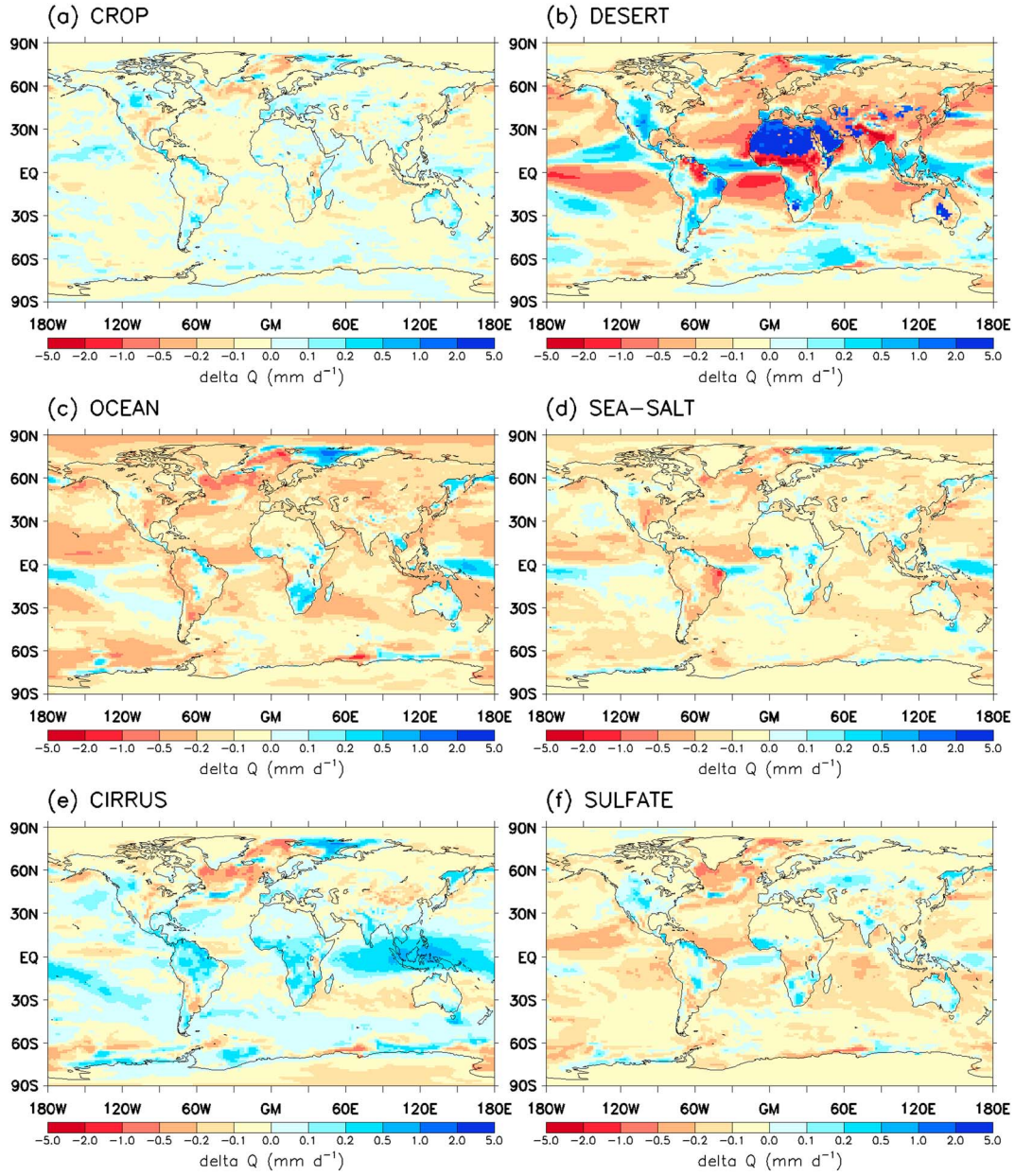

Figure 9. Regional column-integrated diabatic cooling change compared to RCP4.5 (2040–2059) converted to precipitation units (mm d^{-1}) for different geoengineering schemes.

the different nature of the forcing or simply due to internal variability. The decrease in the Amazon was also found for SEA-SALT by *Jones et al.* [2009], and they suggest this comes from the indirect effect in the South Atlantic stratocumulus deck.

The change in column-integrated diabatic cooling, ΔQ, converted into precipitation units is shown for each RM scheme in Figure 9. There is generally a positive correlation between ΔQ and ΔP over land with the mean correlation coefficients for the RM schemes in the range +0.37 to +0.41. There is an anticorrelation over the sea with mean correlation coefficients for the RM schemes in the range −0.40 to −0.42 over the global sea and −0.60 to −0.62 over tropical sea. This suggests diabatic cooling of the atmosphere is largely responsible for precipitation changes over land, but changes in dynamics related to the Hadley cell are responsible for maritime precipitation changes, particularly in the tropics. The correlation is weaker over tropical land where changes in the Hadley cell also affect precipitation.

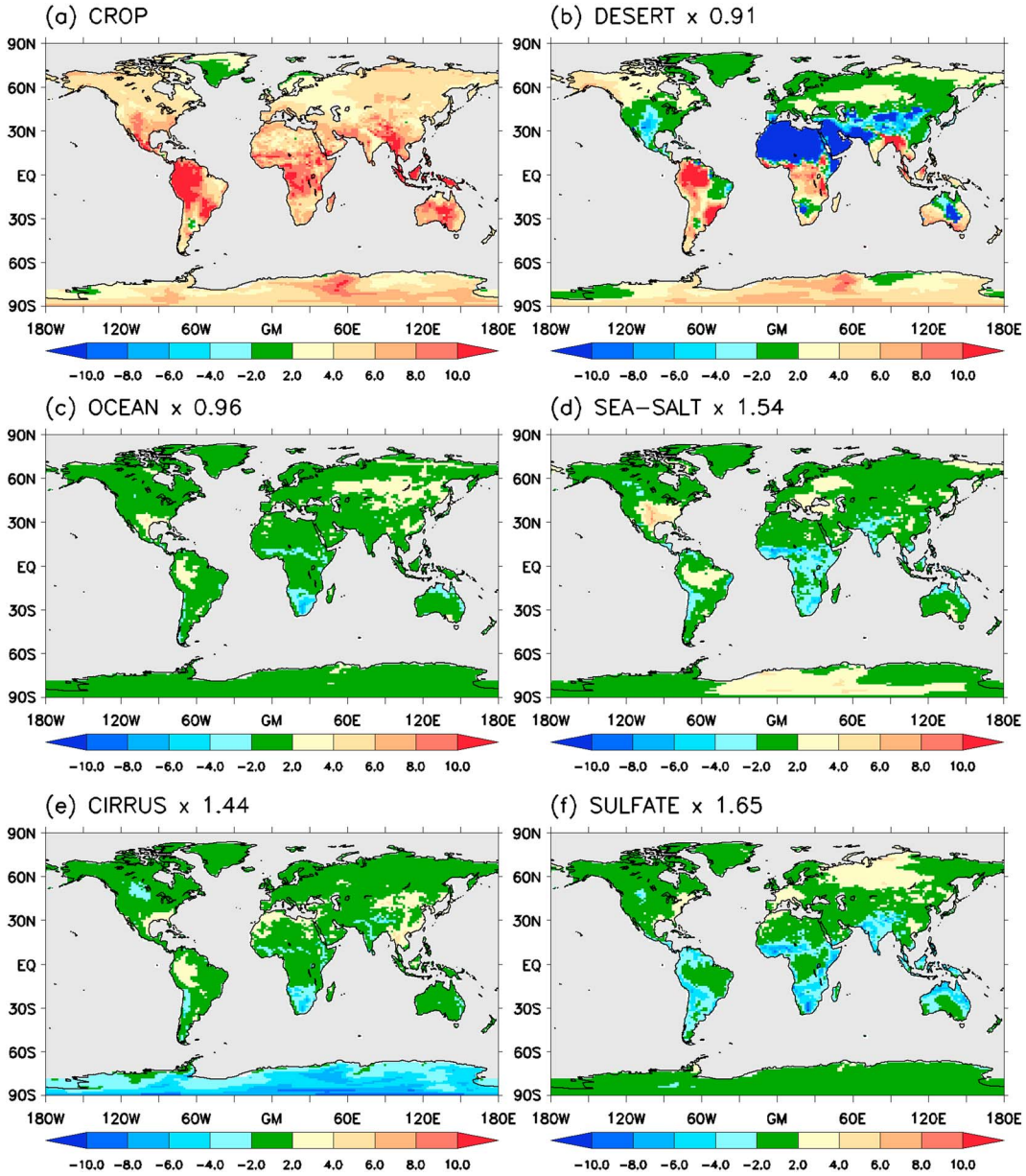

Figure 10. Surface air temperature change (2040–2059) for each geoengineering scheme compared to 1986–2005 climatology expressed as a number of standard deviations (SD20). The temperature difference is bias corrected to bring the global mean temperature back to the climatological mean. Note that CROP geoengineering cannot be scaled up, so bias correction is not performed in this case. The bias correction factors are shown for the other schemes.

3.4.3. After Termination of Geoengineering

Figure 6 shows that over the 5 years after termination, the rates of precipitation change over land for DESERT are more than 10 times greater than the linear rate of change over the whole of the 21st century (0.001 mm d^{-1} yr^{-1}) in RCP4.5. For the other RM schemes the rates of change are only a little greater than the long-term rate of change because the changes due to geoengineering were small. Regionally, much larger rates of change occur on termination (up to 1 mm d^{-1} yr^{-1}). For CIRRUS, the global mean precipitation appears to rapidly reduce and then rebound. Maps of the precipitation difference between geoengineering schemes and RCP4.5 averaged over the 2080–2099 period and expressed as a number of standard deviations (SD20) (Figure S5) show that most of the globe has returned to RCP4.5 within ±2 standard deviations (SD20), and all has returned to within ±4 standard deviations (SD20).

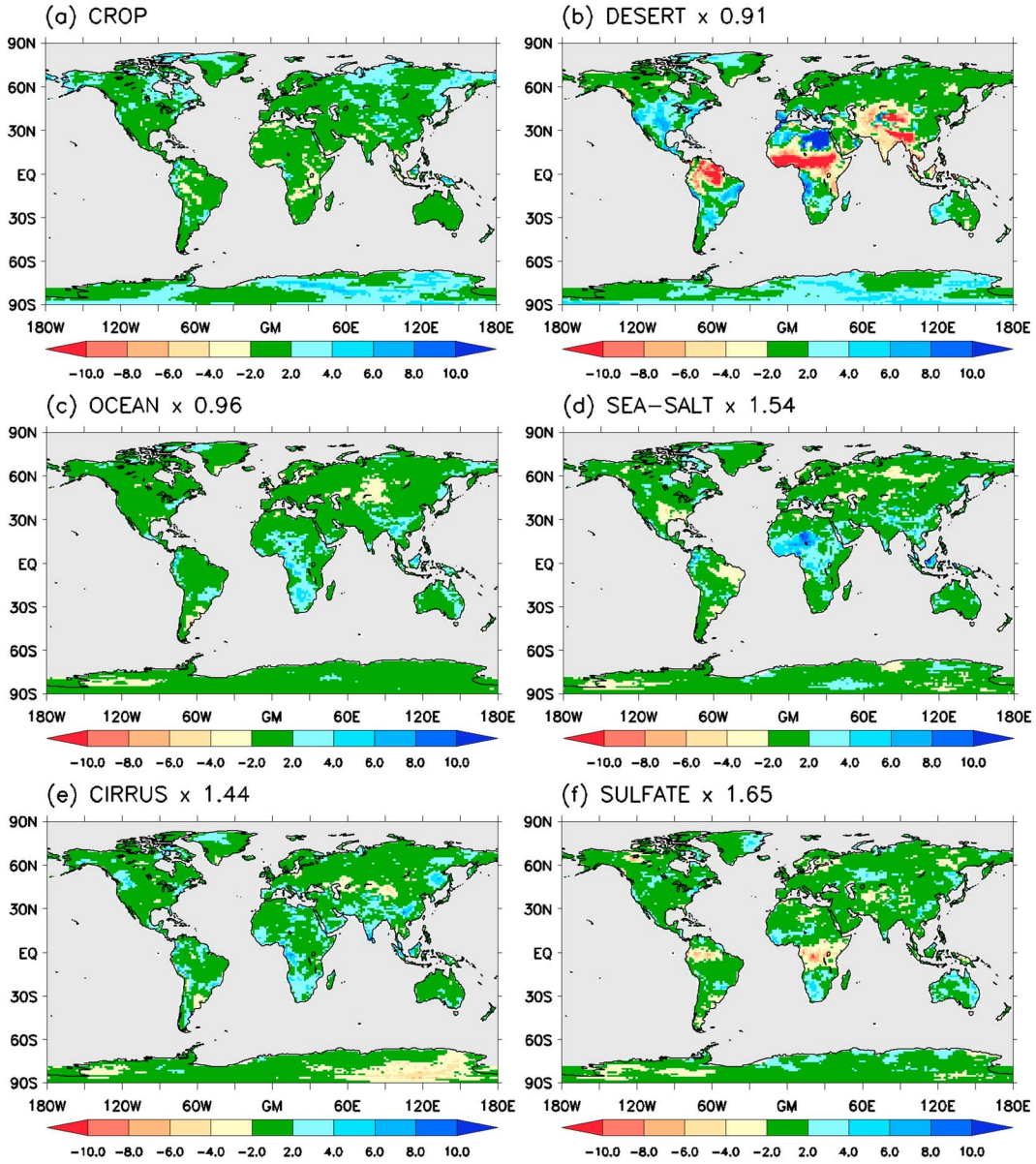

Figure 11. Precipitation change (2040–2059) for each geoengineering scheme compared to 1986–2005 climatology expressed as a number of standard deviations (SD20). The precipitation difference is bias corrected to bring the global mean temperature back to the climatological mean. Note that CROP geoengineering cannot be scaled up, so bias correction is not performed in this case. The bias correction factors are shown for the other schemes.

3.5. Effectiveness

In this section we appraise each RM scheme using a simple assessment framework. Our objective is to provide a more palpable assessment of the impacts of geoengineering than achieved using climate anomaly statistics alone. We define a single target for assessing the RM schemes, returning surface air temperature to its 1986–2005 climatology. To account for natural climate variability, we allow up to two standard deviations variation from the climatological mean. In each grid cell, we assign the response to geoengineering to one of three categories:

1. **Effective**. The climate variable has been brought back within ±2 standard deviations (SD20) of the climatological mean.
2. **Marginally effective**. The climate variable has been brought closer to the climatological mean than RCP4.5 but is still outside ±2 standard deviations (SD20) of the climatological mean.

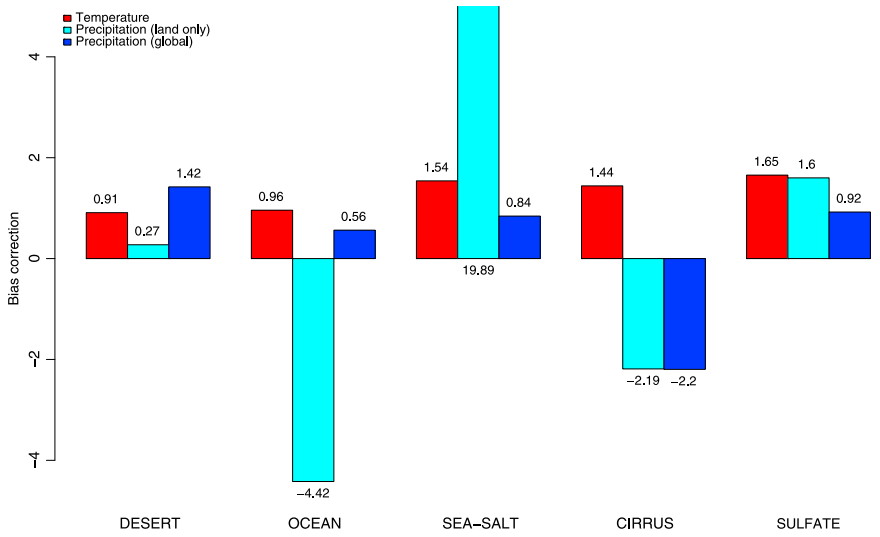

Figure 12. Bias correction factors required to target global mean temperature, global mean precipitation, and mean precipitation over land during the period 2040–2059. The targets are based on a 1986–2005 climatology. Note that the bias correction factor for precipitation over land using SEA-SALT extends beyond the axis range.

3. **Damaging**. The climate variable is now further from the climatological mean (either positive or negative) than RCP4.5.

Our definitions are inevitably subjective, and alternative assessment frameworks have been suggested [e.g., *Ferraro et al.*, 2014a]. Like *Ferraro et al.* [2014a], we do not differentiate between positive and negative deviations from the climatological mean, and our definition of damaging includes both types of deviation. We agree that climate change (e.g., under RCP4.5) will potentially be perceived as beneficial in some regions, to some groups of people or eco-systems. This could potentially be accommodated within an assessment framework by the use of multiple climate targets [e.g., *MacMartin et al.*, 2013] and a wider suite of climate metrics but is beyond the scope of this study. In all cases except CROP, the response has been bias corrected as described in section 2.4.3. The scaling factors used are given in Table 1. The larger the scaling factor used, the further we are extrapolating from our simulation and the greater the caution that should be applied to our conclusions. For CIRRUS, in particular, ERF may not scale linearly with amount of cloud seeding (see section 3.3.1).

Figure 10 shows the mean 2040–2059 surface air temperature of each RM scheme compared to climatology expressed as a number of standard deviations (SD20) and should be compared to RCP4.5 (Figure 1b). CROP is not effective anywhere, leaving temperatures at least 4 standard deviations warmer than climatology over most of the land. It is marginally effective in a few scattered regions. DESERT leaves temperatures more than 10 standard deviations (SD20) cooler than climatology across the desert regions and has an insignificant effect over large parts of northern South America. However, it has effectively cooled parts of Eurasia, southern USA, and Brazil. OCEAN, SEA-SALT, CIRRUS, and SULFATE are effective in many regions but cool too little in parts of Eurasia and cool too much in parts of Africa. However, there are very few places where we would class the temperature change in these geoengineered worlds as damaging.

Figure 11 shows the mean 2040–2059 precipitation intensity of each RM scheme compared to climatology expressed as a number of standard deviations (SD20). CROP has insignificant precipitation change over much of the land. Precipitation intensity for DESERT is more than 10 standard deviations (SD20) away from climatology over a large area of tropical land, with a large percentage of the world population affected. Although the precipitation side effects are less damaging for OCEAN, SEA-SALT, CIRRUS, and SULFATE than for DESERT, these schemes also have a significant area of the world where precipitation is further from climatology than in RCP4.5. None of these RM schemes appears to provide an effective and potentially less damaging precipitation response than the others. It has been suggested that because CIRRUS acts predominantly in the longwave, it may result in precipitation changes that better counteract the changes caused by global warming [*Mitchell and Finnegan*, 2009]. However, we find CIRRUS yielded some damaging changes for regional scale precipitation over land [Figure 11(e)] as did the other RM schemes.

Table 2. Summary of Results

	Description	Scalable to 1.5 K Cooling?	Temperature Response Pattern	Precipitation Response Pattern	Effectiveness
CROP	Increase of albedo for all grasslands (6.2% of the globe) by 0.08.Very small forcing.	No	Cools grasslands and high latitudes but largely insignificant change.	Decreases in grassland areas but largely insignificant change.	Either marginally effective or insignificant temperature response in different regions.
DESERT	Increase of albedo for desert regions (3.6% of the globe) to 0.8. Forcing strongly negative in NH tropics, strongly positive in SH tropics	Yes	Extreme cooling in deserts. Cools NH and warms parts of SH ocean.	Severe shift of ITCZ southward causing severe decrease across NH tropics.	Severely damaging temperature and precipitation responses across large parts of the globe.
OCEAN	Increase of albedo for ice-free oceans by 0.03. Negative forcing extends into extratropics.	Yes	Global cooling. Largely offsets amplified Arctic warming under RCP4.5.		
SEA-SALT	Fixed increase in sea salt aerosol number concentration of 1.8×10^8 m^{-3} between latitudes 30°N–30°S. Negative forcing concentrated in tropics.	Unknown	Global cooling but weaker cooling in Arctic than warming under RCP4.5.	Shift of ITCZ northward increases precipitation north of the equator and decreases it south of the equator.	Widespread regions with damaging precipitation responses, but particularly in Africa.
CIRRUS	Increase in ice crystal fall speed by 4X for air temperatures colder than 233 K. Negative forcing greatest in midlatitudes to high latitudes.	Unlikely	Global cooling but amplified Arctic and Antarctic cooling are greater than the warming under RCP4.5.		
SULFATE	Injection of 10 Tg [SO_2] per year into the tropical lower stratosphere. Negative forcing greatest near the equator.	Unknown	Global cooling but greatest in tropics.		

3.6. Geoengineering to Target Precipitation

Our assessment of geoengineering effectiveness (section 3.5) was based on returning surface air temperature to its global mean 1986–2005 climatology. Precipitation, like temperature, is a climate metric that could be selected as a target for geoengineering. In this section, we consider the impact on global mean temperature and precipitation of targeting the 1986–2005 climatology for global precipitation and mean precipitation over land. We recalculated the bias correction factors using the method described in section 2.4.3, replacing temperature data with the equivalent precipitation data in equations (3) and (4). The bias correction factors are shown in Figure 12: the factors show how each simulated RM scheme would need to be scaled up, or down, to achieve the 1986–2005 climatological mean during 2040–2059; negative values show that the climate would require warming rather than cooling.

Targeting global mean precipitation with OCEAN, SEA-SALT, and SULFATE would require geoengineering to be scaled down compared to the temperature target; this would result in global mean temperatures cooler than RCP4.5 in 2040–2059 but warmer than 1986–2005. In contrast, DESERT geoengineering would require geoengineering to be scaled up and would result in temperatures cooler than 1986–2005.

Targeting mean precipitation over land would require geoengineering to be scaled down for DESERT and scaled up for SULFATE. SEA-SALT has a small impact on precipitation over land, hence its large bias correction factor, and would not be an appropriate RM scheme for targeting mean precipitation over land.

Targeting precipitation over land for OCEAN and targeting precipitation globally or over land for CIRRUS would require a negative scaling, i.e., a warming.

Of the five RM schemes, SULFATE is the only one with similar bias correction

factors for temperature and for precipitation over land. This suggests that SULFATE could simultaneously achieve a close match to both global mean temperature and mean precipitation over land, assuming SULFATE is scalable, although regional variations in temperature and precipitation would remain as previously shown in Figures 10 and 11.

4. Discussion and Conclusions

We compared the impact of six RM methods on global and regional surface air temperature and precipitation, using a fixed amount of geoengineering. Our results are summarized in Table 2. Our precipitation results may seem at odds with the findings of *Kravitz et al.* [2013a] who showed that when a solar constant reduction is used to compensate quadrupling of CO_2 from a pre-industrial control, precipitation remained within ±2 standard deviations of the pre-industrial control. However, those results were for a multimodel mean response and used all models and all years of the pre-industrial control simulations to determine the standard deviation. A multimodel mean response will likely be less extreme than an individual model response, particularly in large parts of Africa and South America where models disagree on the sign of the change. We might expect more damaging precipitation responses from our RM schemes rather than for solar constant reductions. It has been shown that using solar constant reduction gives less damaging precipitation responses than stratospheric SO_2 injection [*Niemeier et al.*, 2013; *Ferraro et al.*, 2014b].

It has been shown, in climate model simulations, that it is possible to control part of the climate system e.g., remediating the Arctic sea ice area using SRM [*Tilmes et al.*, 2014; *Jackson et al.*, 2015]. However, simultaneously limiting precipitation changes would be considerably more difficult than the scenario they illustrated. Potentially damaging changes in regional precipitation were a feature of all our RM schemes.

Our DESERT simulation had a very asymmetric forcing and produced severe shifts in tropical precipitation in line with the findings of *Haywood et al.* [2013]. Our other RM schemes had a more symmetric forcing, yet they still produced shifts in tropical precipitation. Those schemes all had considerably more cooling over the tropical Southern Atlantic than the tropical Northern Atlantic. This suggests that climate model investigations into the sensitivity of tropical precipitation to paired symmetric and asymmetric hemispheric changes would be informative (e.g., changes in hemispheric albedo) [*Voigt et al.*, 2014]. Real world implementation of dynamic geoengineering schemes that manipulate the hemispheric symmetry in forcing would likely be challenging. It would be difficult to determine the required amount of intervention and forcing due to nonlinearity of response as well as lack of understanding of the relationship between the amounts of intervention and forcing.

In this study we limited our analysis to the impact of RM on annual mean surface air temperature and precipitation. Full agricultural impact assessments indicating damage to crop yields, and impacts on flooding require smaller scale analysis and are beyond the scope of this study. RCP4.5 assumes that some mitigation will occur. However, should significantly less mitigation occur than in RCP4.5, it would be unlikely that any of our RM schemes in isolation could restore the climate to its 1986–2005 state. Finally, our simulations were performed with a single climate model. Comparisons of RM schemes in different models will confirm whether our conclusions are robust.

Acknowledgments
We thank all participants on the Integrated Assessment of Geo-engineering Proposals (IAGP) project and acknowledge the financial support under grant EP/I014721/1 from the Engineering and Physical Sciences Research Council (EPSRC) and Natural Environment Research Council (NERC). P.F. was also supported by a Royal Society Wolfson Merit Award. S.O. was supported under the EPSRC funded SPICE project. This work made use of HECToR and ARCHER, the UK's national high-performance computing service, provided by UoE HPCx Ltd at the University of Edinburgh, Cray Inc, and NAG Ltd, and the JWCRP owned and administered MONSooN computing facility. We gratefully acknowledge the reviewers for comments and suggestions that greatly improved the manuscript. Model data are available on request from J.A.C.

References

Albrecht, B. A. (1989), Aerosols, cloud microphysics, and fractional cloudiness, *Science*, *245*, 1227–1230.

Alterskjær, K., J. E. Kristjánsson, O. Boucher, H. Muri, U. Niemeier, H. Schmidt, M. Schulz, and C. Timmreck (2013), Sea-salt injections into the low-latitude marine boundary layer: The transient response in three Earth system models, *J. Geophys. Res. Atmos.*, *118*, 12,195–12,206, doi:10.1002/2013JD020432.

Andrews, T., P. M. Forster, and J. M. Gregory (2009), A surface energy perspective on climate change, *J. Clim.*, *22*, 2557–2570, doi:10.1175/2008JCLI2759.1.

Bala, G., P. B. Duffy, and K. E. Taylor (2008), Impact of geoengineering schemes on the global hydrological cycle, *Proc. Natl. Acad. Sci. U.S.A.*, *105*, 7664–7669, doi:10.1073/pnas.0711648105.

Bellouin, N., O. Boucher, J. Haywood, C. Johnson, A. Jones, J. Rae, and S. Woodward (2007), Improved representation of aerosols for HadGEM2, Hadley Centre Technical Note 73, Met Office Hadley Centre for Climate Change, Exeter, U. K.

Boucher, O., P. M. Forster, N. Gruber, M. Ha-Duong, M. G. Lawrence, T. M. Lenton, A. Maas, and N. E. Vaughan (2014), Rethinking climate geoengineering categorisation in the context of climate change mitigation and adaptation, *WIREs Clim. Change*, *5*, 23–35, doi:10.1002/wcc.261.

Budyko, M. I. (1977), *Climatic Changes*, 261 pp., AGU, Washington, D. C., doi:10.1029/SP010.

Collins, M., et al. (2013), Long-term climate change: Projections, commitments and irreversibility, in *Climate Change 2013: The Physical Science Basis. Contribution of Working Group I to the Fifth Assessment Report of the Intergovernmental Panel on Climate Change*, edited by T. F. Stocker et al., Cambridge Univ. Press, Cambridge, U. K., and New York.

Cox, P. M. (2001), Description of the "TRIFFID" dynamic global vegetation model, Hadley Centre Technical Note 24. Met Office, Exeter, U. K.

Crook, J. A., P. M. Forster, and N. Stuber (2011), Spatial patterns of modeled climate feedback and contributions to temperature response and polar amplification, *J. Clim.*, *24*, 3575–3592, doi:10.1175/2011JCLI3863.1.

Crutzen, P. (2006), Albedo enhancement by stratospheric sulphur injections: A contribution to resolve a policy dilemma?, *Clim. Change*, *77*, 211–219, doi:10.1007/s10584-006-9101-y.

Doughty, C. E., C. B. Field, and A. M. S. McMillan (2011), Can crop albedo be increased through the modification of leaf trichomes, and could this cool regional climate?, *Clim. Change*, *104*(2), 379–387, doi:10.1007/s10584-010-9936-0.

Essery, R., M. Best, and P. Cox (2001), MOSES 2.2 technical documentation, HadleyCentre Technical Note 30. Met Office, Exeter, U. K.

Evans, J. G. R., E. P. J. Stride, M. J. Edirisinghe, D. J. Andrews, and R. R. Simons (2010), Can oceanic foams limit global warming?, *Clim. Res.*, *42*, 155–160, doi:10.3354/cr00885.

Ferraro, A. J., A. J. Charlton-Perez, and E. J. Highwood (2014a), A risk-based framework for assessing the effectiveness of stratospheric aerosol geoengineering, *PLoS One*, *9*(2), e88849, doi:10.1371/journal.pone.0088849.

Ferraro, A. J., E. J. Highwood, and A. J. Charlton-Perez (2014b), Weakened tropical circulation and reduced precipitation in response to geoengineering, *Environ. Res. Lett.*, *9*, 014001, doi:10.1088/1748-9326/9/1/014001.

Gaskill, A. (2004), Summary of meeting with US DOE to discuss geoengineering options to prevent long-term climate change, Environ. Ref. Mater., Inc., Research Triangle Park, N. C.

Gregory, J. M., W. J. Ingram, M. A. Palmer, G. S. Jones, P. A. Stott, R. B. Thorpe, J. A. Lowe, T. C. Johns, and K. D. Williams (2004), A new method for diagnosing radiative forcing and climate sensitivity, *Geophys. Res. Lett.*, *31*, L03205, doi:10.1029/2003GL018747.

Hardiman, S. C., N. Butchart, T. J. Hinton, S. M. Osprey, and L. J. Gray (2012), The effect of a well-resolved stratosphere on surface climate: Differences between CMIP5 simulations with high and low top versions of the met office climate model, *J. Clim.*, *25*(20), 7083–7099, doi:10.1175/JCLI-D-11-00579.1.

Haywood, J. M., A. Jones, N. Bellouin, and D. Stephenson (2013), Asymmetric forcing from stratospheric aerosols impacts Sahelian rainfall, *Nat. Clim. Change*, *3*, 660–665, doi:10.1038/NCLIMATE1857.

Heckendorn, P., D. Weisenstein, S. Fueglistaler, B. P. Luo, E. Rozanov, M. Schraner, L. W. Thomason, and T. Peter (2009), The impact of geoengineering aerosols on stratospheric temperature and ozone, *Environ. Res. Lett.*, *4,* 045108, doi:10.1088/1748-9326/4/4/045108.

Intergovernmental Panel on Climate Change (2013), Summary for policymakers, in *Climate Change 2013: The Physical Science Basis. Contribution of Working Group I to the Fifth Assessment Report of the Intergovernmental Panel on Climate Change*, edited by T. F. Stocker et al., Cambridge Univ. Press, Cambridge, U. K., and New York.

Irvine, P. J., A. Ridgwell, and D. J. Lunt (2011), Climatic effects of surface albedo geoengineering, *J. Geophys. Res.*, *116*, D24112, doi:10.1029/2011JD016281.

Jackson, L. S., J. A. Crook, A. Jarvis, D. Leedal, A. Ridgwell, N. Vaughan, and P. M. Forster (2015), Assessing the controllability of Arctic sea ice extent by sulfate aerosol geoengineering, *Geophys. Res. Lett.*, *41*, 1223–1231, doi:10.1002/2014GL062240.

Jones, A., and J. M. Haywood (2012), Sea-spray geoengineering in the HadGEM2-ES earth-system model: Radiative impact and climate response, *Atmos. Chem. Phys.*, *12*, 10,887–10,898, doi:10.5194/acp-12-10887-2012.

Jones, A., D. L. Roberts, M. J. Woodage, and C. E. Johnson (2001), Indirect sulphate aerosol forcing in a climate model with an interactive sulphur cycle, *J. Geophys. Res.*, *106*(D17), 20,293–29,310, doi:10.1029/2000JD000089.

Jones, A., J. Haywood, and O. Boucher (2009), Climate impacts of geoengineering marine stratocumulus clouds, *J. Geophys. Res.*, *114*, D10106, doi:10.1029/2008JD011450.

Jones, A., J. Haywood, O. Boucher, B. Kravitz, and A. Robock (2010), Geoengineering by stratospheric SO_2 injection: Results from the Met Office HadGEM2 climate model and comparison with the Goddard Institute for Space Studies ModelE, *Atmos. Chem. Phys.*, *10*, 5999–6006, doi:10.5194/acp-10-5999-2010.

Jones, A., J. M. Haywood, and O. Boucher (2011), A comparison of the climate impacts of geoengineering by stratospheric SO_2 injection and by brightening of marine stratocumulus cloud, *Atmos. Sci. Lett.*, *12*, 176–183, doi:10.1002/asl.291.

Jones, A., et al. (2013), The impact of abrupt suspension of solar radiation management (termination effect) in experiment G2 of the Geoengineering Model Intercomparison Project (GeoMIP), *J. Geophys. Res. Atmos.*, *118*, 9743–9752, doi:10.1002/jgrd.50762.

Kalidindi, S., G. Bala, A. Modak, and K. Caldeira (2015), Modeling of solar radiation management: A comparison of simulations using reduced solar constant and stratospheric sulphate aerosols, *Clim. Dyn.*, doi:10.1007/s00382-014-2240-3.

Karcher, B., and U. Lohmann (2002), A parameterization of cirrus cloud formation: Homogeneous freezing of supercooled aerosols, *J. Geophys. Res.*, *107*, D2, 4010, doi:10.1029/2001JD000470.

Keith, D. W. (2000), Geoengineering the climate: History and prospect, *Annu. Rev. Energy Environ.*, *25*, 245–84.

Kravitz, B., A. Robock, O. Boucher, H. Schmidt, K. E. Taylor, G. Stenchikov, and M. Schulz (2011), The Geoengineering Model Intercomparison Project (GeoMIP), *Atmos. Sci. Lett.*, *12*, 162–167, doi:10.1002/asl.316.

Kravitz, B., et al. (2013a), Climate model response from the Geoengineering Model Intercomparison Project (GeoMIP), *J. Geophys. Res. Atmos*, *118*, 8320–8332, doi:10.1002/jgrd.50646.

Kravitz, B., et al. (2013b), Sea spray geoengineering experiments in the geoengineering model intercomparison project (GeoMIP): Experimental design and preliminary results, *J. Geophys. Res. Atmos.*, *118*, 11,175–11,186, doi:10.1002/jgrd.50856.

Latham, J. (1990), Control of global warming?, *Nature*, *347*, 339–340.

Latham, J., P. Rasch, C.-C. Chen, L. Kettles, A. Gadian, A. Gettelman, H. Morrison, K. Bower, and T. Choularton (2008), Global temperature stabilization via controlled albedo enhancement of low-level maritime clouds, *Philos. Trans. R. Soc. London, Ser. A*, *366*, 3969–3987, doi:10.1098/rsta.2008.0137.

Lenton, T. M., and N. E. Vaughan (2009), The radiative forcing potential of different climate geoengineering options, *Atmos. Chem. Phys.*, *9*, 5539–5561.

MacMartin, D. G., D. W. Keith, B. Kravitz, and K. Caldeira (2013), Management of trade-offs in geoengineering through optimal choice of non-uniform radiative forcing, *Nat. Clim. Change*, *3*, 365–368, doi:10.1038/nclimate1722.

Martin, G. M., et al. (2011), The HadGEM2 family of Met Office Unified Model climate configurations, *Geosci. Model Dev.*, *4*, 723–757, doi:10.5194/gmd-4-723-2011.

Mitchell, D. L. (1996), Use of mass- and area-dimensional power laws for determining precipitation particle terminal velocities, *J. Atmos. Sci.*, *53*, 1710–1723.

Mitchell, D. L., and W. Finnegan (2009), Modification of cirrus clouds to reduce global warming, *Environ. Res. Lett.*, *4*, 045102, doi:10.1088/1748-9326/4/4/045102.

Mitchell, D. L., P. Rasch, D. Ivanova, G. McFarquhar, and T. Nousiainen (2008), Impact of small ice crystal assumptions on ice sedimentation rates in cirrus clouds and GCM simulations, *Geophys. Res. Lett.*, *35*, L09806, doi:10.1029/2008GL033552.

Moore, K. D., K. V. Voss, and H. R. Gordon (2000), Spectral reflectance of whitecaps: Their contribution to water-leaving radiance, *J. Geophys. Res.*, *105*(C3), 6493–6499, doi:10.1029/1999JC900334.

Moss, R. H., et al. (2010), The next generation of scenarios for climate change research and assessment, *Nature*, *463*, 747–756, doi:10.1038/nature08823.

Muller, C. J., and P. A. O'Gorman (2011), An energetic perspective on the regional response of precipitation to climate change, *Nat. Clim. Change*, *1*, 266–271, doi:10.1038/NCLIMATE1169.

Muri, H., J. E. Kristjansson, T. Storelvmo, and M. A. Pfeffer (2014), The climatic effects of modifying cirrus clouds in a climate engineering framework, *J. Geophys. Res. Atmos.*, *119*, 4174–4191, doi:10.1002/2013JD021063.

Myhre, G., et al. (2013), Anthropogenic and natural radiative forcing, in *Climate Change 2013: The Physical Science Basis. Contribution of Working Group I to the Fifth Assessment Report of the Intergovernmental Panel on Climate Change*, edited by T. F. Stocker et al., Cambridge Univ. Press, Cambridge, U. K., and New York.

Niemeier, U., H. Schmidt, and C. Timmreck (2011), The dependency of geoengineered sulfate aerosol on the emission strategy, *Atmos. Sci. Lett.*, *12*, 189–194, doi:10.1002/asl.304.

Niemeier, U., H. Schmidt, K. Alterskjær, and J. E. Kristjánsson (2013), Solar irradiance reduction via climate engineering: Impact of different techniques on the energy balance and the hydrological cycle, *J. Geophys. Res. Atmos.*, *118*, 11,905–11,917, doi:10.1002/2013JD020445.

Ridgwell, A., J. S. Singarayer, A. M. Hetherington, and P. J. Valdes (2009), Tackling regional climate change by leaf albedo bio-geoengineering, *Curr. Biol.*, *19*, 146–150, doi:10.1016/j.cub.2008.12.025.

Robock, A. (2000), Volcanic eruptions and climate, *Rev. Geophys.*, *38*, 191–219, doi:10.1029/1998RG000054.

Salter, S., G. Sortino, and J. Latham (2008), Sea-going hardware for the cloud albedo method of reversing global warming, *Philos. Trans. R. Soc. London, Ser. A*, *366*(1882), 3989–4006.

Sanderson, B. M., C. Piani, W. J. Ingram, D. A. Stone, and M. R. Allen (2008), Towards constraining climate sensitivity by linear analysis of feedback patterns in thousands of perturbed-physics GCM simulations, *Clim. Dyn.*, *30*, 175–190, doi:10.1007/s00382-007-0280-7.

Seitz, R. (2011), Bright water: Hydrosols, water conservation and climate change, *Clim. Change*, *105*, 365–381, doi:10.1007/s10584-010-9965-8.

Shepherd, J. G. (2012), Geoengineering the climate: An overview and update, *Philos. Trans. R. Soc. London, Ser. A*, *370*, 4166–4175, doi:10.1098/rsta.2012.0186.

Singarayer, J. S., A. Ridgwell, and P. Irvine (2009), Assessing the benefits of crop albedo bio-geoengineering, *Environ. Res. Lett.*, *4*, 045110, doi:10.1088/1748-9326/4/4/045110.

Storelvmo, T., J. E. Kristjansson, H. Muri, M. Pfeffer, D. Barahona, and A. Nenes (2013), Cirrus cloud seeding has potential to cool climate, *Geophys. Res. Lett.*, *40*, 178–182, doi:10.1029/2012GL054201.

Taylor, K. E., R. J. Stouffer, and G. A. Meehl (2012), An overview of CMIP5 and the experiment design, *Bull. Am. Meteorol. Soc.*, *93*, 485–498, doi:10.1175/BAMS-D-11-00094.1.

Thomson, A. M., et al. (2011), RCP4.5: A pathway for stabilization of radiative forcing by 2100, *Clim. Change*, *109*, 77–94, doi:10.1007/s10584-011-0151-4.

Tilmes, S., et al. (2013), The hydrological impact of geoengineering in the Geoengineering Model Intercomparison Project (GeoMIP), *J. Geophys. Res. Atmos.*, *118*, 11,036–11,058, doi:10.1002/jgrd.50868.

Tilmes, S., A. Jahn, J. E. Kay, M. Holland, and J.-F. Lamarque (2014), Can regional climate engineering save the summer Arctic sea ice?, *Geophys. Res. Lett.*, *41*, 880–885, doi:10.1002/2013GL058731.

Twomey, S. (1977), Influence of pollution on shortwave albedo of clouds, *J. Atmos. Sci.*, *34*, 1149–1152, doi:10.1175/1520-0469(1977)034<1149:TIOPOT>2.0.CO;2.

Vaughan, N. E., and T. M. Lenton (2011), A review of climate geoengineering proposals, *Clim. Change*, *109*, 745–790, doi:10.1007/s10584-011-0027-7.

Voigt, A., B. Stevens, J. Bader, and T. Mauritsen (2014), Compensation of hemispheric albedo asymmetries by shifts of the ITCZ and tropical clouds, *J. Clim.*, *27*, 1029–1045, doi:10.1175/JCLI-D-13-00205.1.

Wilson, D. R., and S. P. Ballard (1999), A microphysically based precipitation scheme for the UK Meteorological Office Unified Model, *Q. J. R. Meteorol. Soc.*, *125*, 1607–1636.

Yu, X., J. C. Moore, X. Cui, A. Rinke, D. Ji, B. Kravitz, and J.-H. Yoon (2015), Impacts, effectiveness and regional inequalities of the GeoMIP G1 to G4 solar radiation management scenarios, *Global Planet. Change*, *129*, 10–22.